

JDC FILE COPY

AD A058607

UNCLASSIFIED

SECURITY CLASSIFICATION OF THIS PAGE (When Data Entered)

| REPORT DOCUMENTATION PAGE | | READ INSTRUCTIONS BEFORE COMPLETING FORM |
|--|-----------------------|---|
| 1. REPORT NUMBER TR-3804 | 2. GOVT ACCESSION NO. | 3. RECIPIENT'S CATALOG NUMBER |
| 4. TITLE (and Subtitle) PULSE CHARGING OF NANOFARAD CAPACITORS TO TENS OF KILOVOLTS FROM THE SHOCK DEPOLING OF PZT FERROELECTRIC CERAMICS | | 5. TYPE OF REPORT & PERIOD COVERED Final rept. |
| 7. AUTHOR(s) W. Mock, Jr. W. H. Holt | | 6. PERFORMING ORG. REPORT NUMBER |
| 9. PERFORMING ORGANIZATION NAME AND ADDRESS Naval Surface Weapons Center (G30) Dahlgren, Virginia 22448 | | 8. CONTRACT OR GRANT NUMBER(s) F32382 |
| 11. CONTROLLING OFFICE NAME AND ADDRESS Naval Air Systems Command Washington, DC 20360 | | 10. PROGRAM ELEMENT, PROJECT, TASK AREA & WORK UNIT NUMBERS 62332N/S32382/ WF32382501/DF29 |
| 14. MONITORING AGENCY NAME & ADDRESS (if different from Controlling Office) | | 12. REPORT DATE Apr 78 |
| | | 13. NUMBER OF PAGES 80 |
| | | 15. SECURITY CLASS. (of this report) UNCLASSIFIED |
| | | 15a. DECLASSIFICATION/DOWNGRADING SCHEDULE |
| 16. DISTRIBUTION STATEMENT (of this Report) Approved for public release; distribution unlimited. | | |
| 17. DISTRIBUTION STATEMENT (of the abstract entered in Block 20, if different from Report) | | |
| 18. SUPPLEMENTARY NOTES | | |
| 19. KEY WORDS (Continue on reverse side if necessary and identify by block number) Ferroelectric Ceramics Ferroelectric Power Supply Shock Waves Pulsed High Voltage Gas Gun Pulse Power Shock-Depoled Ferroelectrics Dielectric Properties | | |
| 20. ABSTRACT (Continue on reverse side if necessary and identify by block number) Gas gun impact techniques have been used to pulse charge nanofarad capacitors from the shock depoling of PZT 56/44 and PZT 95/5 ferroelectric ceramics. The PZT materials were depoled in the normal mode. Pulse powers of hundreds of kilowatts were produced in a few microseconds. The PZT 56/44 material was impacted in the stress range from 4.4 to 11.8 GPa. A maximum load voltage of 55 kV was produced at 7.9 GPa. Shock-induced electrical breakdown in the PZT material occurred at 11.8 GPa. The PZT 95/5 material was impacted at 1.4 and 2.9 GPa stress levels. A maximum load voltage of 81 kV was produced at the higher stress. | | |

DD FORM 1 JAN 73 1473

EDITION OF 1 NOV 65 IS OBSOLETE
S/N 0102-014-6601

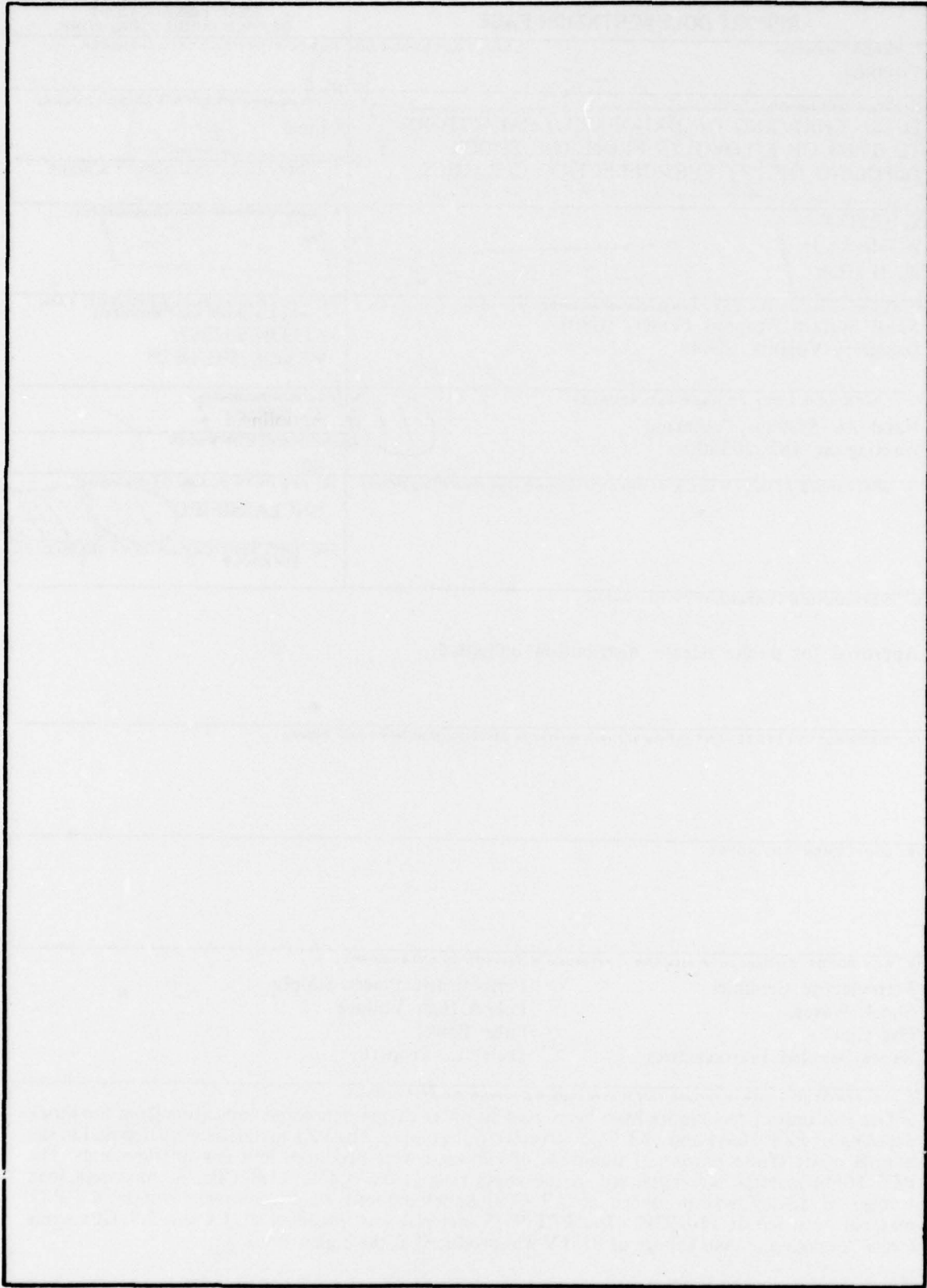
UNCLASSIFIED

SECURITY CLASSIFICATION OF THIS PAGE (When Data Entered)

391 598

UNCLASSIFIED

SECURITY CLASSIFICATION OF THIS PAGE(When Data Entered)



UNCLASSIFIED

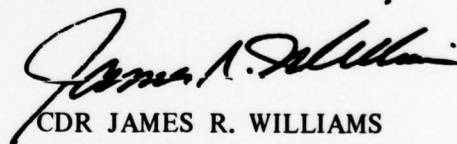
SECURITY CLASSIFICATION OF THIS PAGE(When Data Entered)

FOREWORD

The high voltage electrical properties of PZT 56/44 and PZT 95/5 ferroelectric ceramics have been investigated under normal-mode shock depoling. These properties are important for applications involving single-shot ferroelectric pulse power supplies. Funding for this work was provided by NAVAIR Task No. A350-3500/004C/6WTW27-001.

This report has been reviewed by C. A. Cooper, Head, Gun Systems and Munitions Division.

Released by:



CDR JAMES R. WILLIAMS
Assistant Head for Weapons Systems
Weapons Systems Department

| | |
|------------------------------------|---|
| ACCESSION for | |
| NTIS | White Section <input checked="" type="checkbox"/> |
| DDC | Buff Section <input type="checkbox"/> |
| UNANNOUNCED | |
| JUSTIFICATION | |
| BY DISTRIBUTION/AVAILABILITY CODES | |
| Dist. | Special |
| A | |

ACKNOWLEDGEMENT

The authors would like to thank P. C. Lysne of Sandia Laboratories for helpful discussions and comments concerning this report.

TABLE OF CONTENTS

| | <u>Page</u> |
|--|-------------|
| FOREWORD | iii |
| ACKNOWLEDGEMENT | iv |
| LIST OF ILLUSTRATIONS | vi |
| LIST OF TABLES | viii |
| I. INTRODUCTION | 1 |
| II. PZT MATERIALS | 2 |
| III. EXPERIMENTAL TECHNIQUES | 4 |
| IV. PZT TARGET ASSEMBLY FABRICATION | 13 |
| V. SIMPLIFIED MODEL | 21 |
| VI. RESULTS AND DISCUSSION | 26 |
| VII. SUMMARY | 41 |
| REFERENCES | 42 |
| APPENDIXES | |
| A - DISCUSSION OF ELECTRICAL EQUATIONS FOR THE IDEAL RESPONSE OF A PZT UNIT WITH A CAPACITIVE LOAD | A-1 |
| B - VOLTAGE AND CURRENT OSCILLOSCOPE RECORDS | B-1 |
| DISTRIBUTION | |

LIST OF ILLUSTRATIONS

| <u>Figure</u> | <u>Page</u> |
|--|-------------|
| 1 Schematic of PZT element | 3 |
| 2 Schematic of experimental arrangement for generating and measuring released charge and voltage from shock-depoled PZT unit. | 5 |
| 3 Schematic of muzzle region of gas gun showing the details of the target assembly for normal-voltage-mode depoling of PZT material. | 5 |
| 4 PZT target assembly on gas gun muzzle prior to firing gun. | 8 |
| 5 High voltage box showing the resistive voltage probe (at the end of the box) and the current probe (in the middle of the box). | 8 |
| 6 High voltage box with the lid raised showing the electrical components in the box. | 10 |
| 7 PZT elements and brass electrodes prior to assembly into a unit. | 13 |
| 8 PZT unit compressively held in a hinged-beam clamp during conductive epoxy cure. | 14 |
| 9 Completed PZT unit. | 15 |
| 10 PZT unit and trigger pin positioned on brass fixture prior to insertion into Lucite target holder. | 16 |
| 11 Experimental arrangement for measuring the distance between the impact plane of the target assembly and the PZT unit. | 17 |
| 12 Target holder with brass fixture containing PZT unit and trigger pin on granite surface plate prior to first epoxy pour. | 18 |
| 13 Target assembly showing PZT unit and attached trigger pin cable after first epoxy pour and removal of brass fixture. | 19 |
| 14 Completed PZT target assembly. | 20 |
| 15 Schematic of the normal-voltage-mode depoling of a PZT unit with a capacitive load. | 22 |
| 16 Schematic of voltage and current pulses for the normal mode depoling of a PZT unit. | 24 |
| 17 Voltage pulse for PZT 56/44 unit in Shot 71. | 28 |
| 18 Voltage and current pulses for PZT 56/44 unit in Shot 83. | 28 |
| 19 Voltage and current pulses for PZT 56/44 unit in Shot 84. | 29 |

LIST OF ILLUSTRATIONS (Continued)

| <u>Figure</u> | | <u>Page</u> |
|---------------|---|-------------|
| 20 | Voltage and current pulses for PZT 56/44 unit in Shot 85. | 29 |
| 21 | Voltage and current pulses for PZT 56/44 unit in Shot 87. | 30 |
| 22 | Voltage and current pulses for PZT 56/44 unit in Shot 121. | 30 |
| 23 | Voltage and current pulses for PZT 95/5 unit in Shot 122. | 31 |
| 24 | Voltage and current pulses for PZT 95/5 unit in Shot 123. | 31 |
| 25 | Voltage pulses as a function of shock stress for identical PZT 56/44 units. | 37 |
| 26 | Released charge as a function of shock stress for identical PZT 56/44 units. | 37 |
| 27 | Effect of doubling the charge available for release on the voltage output for PZT 56/44 units. | 38 |
| 28 | Voltage pulses for PZT 95/5 units. | 38 |
| A-1 | Normalized charge and voltage on the PZT unit for various values of the C_L/C ratio. | A-4 |
| A-2 | Normalized circuit current for various values of the C_L/C ratio. | A-5 |
| A-3 | Normalized energy on the PZT unit for various values of the C_L/C ratio. | A-7 |
| A-4 | Normalized energy on the load capacitor for various values of the C_L/C ratio. | A-7 |
| A-5 | Normalized circuit energy for various values of the C_L/C ratio. | A-8 |
| B-1 | Voltage record for Shot 71. | B-3 |
| B-2 | Voltage and current records for Shot 83. | B-4 |
| B-3 | Voltage and current records for Shot 84. | B-5 |
| B-4 | Voltage and current records for Shot 85. | B-6 |
| B-5 | Voltage and current records for Shot 87. | B-7 |
| B-6 | Voltage and current records for Shot 121. | B-8 |
| B-7 | Voltage and current records for Shot 122. | B-9 |
| B-8 | Voltage and current records for Shot 123. | B-10 |

LIST OF TABLES

| <u>Table</u> | <u>Page</u> |
|---|-------------|
| 1 Average piezoelectric and ferroelectric properties of PZT elements (Reference 12). | 3 |
| 2 Density and size of PZT elements and units. | 6 |
| 3 Ferroelectric and dielectric properties of PZT units. | 7 |
| 4 National Bureau of Standards calibration results for T&M resistive voltage probes. | 11 |
| 5 Voltage and current probes used for each shot. | 12 |
| 6 Projectile and target impact parameters. | 13 |
| 7 Summary of voltage measurements for shock-depoled PZT units. | 27 |
| 8 Comparison of voltage and current probe measurements of charge transferred to capacitive load. | 33 |
| 9 Comparison of maximum current measurements and calculations from voltage pulses. | 34 |
| 10 Comparison of voltage measurements for the shock-depoled PZT units with calculations for the theoretical maximum voltage assuming ideal units. | 35 |
| 11 Summary of ultrasonic velocity measurements. | 40 |

I. INTRODUCTION

Ferroelectric materials are polar crystals whose dipole moments can be reversed by an applied electric field. These materials are characterized by a hysteresis loop of the polarization vector versus the applied electric field. Lead zirconate titanate (PZT) ceramics are ferroelectric materials that have found wide application in recent years because of their superior piezoelectric properties. When poled, these materials exhibit a strong coupling between electrical and mechanical properties. They are used as reversible generators of electrical energy in the fields of acoustics and ultrasonics. Examples of piezoelectric PZT devices are phonographic pickups, delay lines, and wave filters.¹

PZT materials have also been used as elements in shock-wave-actuated power supplies. In this mode of operation the surface charge is released from the poled PZT ceramic as the shock stress passes through it. The compressive stresses attained in the shock environment usually exceed the linear piezoelectric limit of the material. Past work has shown that the charge release is a complicated function of the shock stress.^{2,3} It has been concluded that in some PZT materials the depoling is due to a reorientation of the ferroelectric domains and in other materials it is due to a shock-induced phase transition.⁴⁻⁶ In addition, the depoling phenomenon is complicated by dielectric breakdown in the PZT material when the shock stresses and generated electric fields exceed critical values.^{2,7,8}

Most of the published investigations of charge release phenomena under shock wave compression have been performed for either short circuit conditions or very large resistive loads.^{3,9,10} We present in this report the results of an investigation of the shock depoling of PZT elements with a capacitive load. Two PZT ceramic materials having different compositions were investigated. The load voltage and circuit current were used to monitor the electromechanical response of the materials. The charge transferred to the capacitive load was calculated from both the voltage and current histories. Results are presented for a fixed size PZT unit as a function of increasing shock stress to determine if a stress range exists for optimum charge release. Also, some shots were made at the same shock stress on different size PZT units to determine if the charge release scales with the size of the unit.

The piezoelectric and ferroelectric properties of the PZT ceramics used in this study are presented in the next section. A discussion of the experimental techniques used for producing the shock stresses and measuring the load voltage and circuit current are given in Section III. The details of the PZT target assembly fabrication

procedure are presented in Section IV. In Section V a simplified model is presented for the normal-mode shock depoling of the PZT unit with a capacitive load. The experimental results are presented and discussed in Section VI. The work is summarized in Section VII. In Appendix A the simplified model is discussed in terms of the load to source capacitance ratio. Appendix B contains the voltage and current oscilloscope records.

II. PZT MATERIALS

PZT 56/44 and PZT 95/5 are the two ferroelectric ceramic materials used in this investigation.¹¹ PZT 56/44 is a solid solution containing 56 mole % lead zirconate and 44 mole % lead titanate with the minor added constituents of niobium, strontium, and lanthanum. The material was normal fired at 1280°C for 3 hr. The Curie point for this composition is greater than 240°C. This composition is located near the rhombohedral-tetragonal phase boundary of the PbZrO_3 and PbTiO_3 phase diagram and is characterized by strong piezoelectric effects.¹ It was not possible to hydrostatically depole this material completely for stresses up to 0.48 GPa although partial depoling occurred.¹² The average density for eight pieces from three different sizes of PZT elements was 7.58 Mg/m³.

PZT 95/5 is a solid solution containing 95 mole % lead zirconate and 5 mole % lead titanate with niobium as a minor added constituent. The chemical formula is $\text{Pb}_{0.9925}\text{Nb}_{0.015}(\text{Zr}_{0.95}\text{Ti}_{0.05})_{0.985}\text{O}_3$. Approximately 0.6 mole % silicon dioxide was added to control the magnitude of the polarization vector. This constituent goes into the grain boundaries of the PZT ceramic. The material was normal fired at 1345°C for 4.5 hr. This composition is located near the orthorhombic antiferroelectric PbZrO_3 phase boundary and has a Curie point of approximately 240°C. It was hydrostatically depoled completely with a stress of 0.29 GPa.¹² The average density for three pieces of a single size element was 7.47 Mg/m³.

Figure 1 is a schematic of a poled PZT element showing the direction of the polarization vector. Table 1 lists some of the piezoelectric and ferroelectric parameters for PZT 56/44 and PZT 95/5. K_3 is the low frequency dielectric constant in the polarization direction. The piezoelectric voltage and charge coefficients are, respectively, the ratios of the electric field and generated charge to the stress applied in the polarization direction. They are related through the equation $d_{33} = K_3 a_0 g_{33}$ where ϵ_0 is the permittivity of free space. These

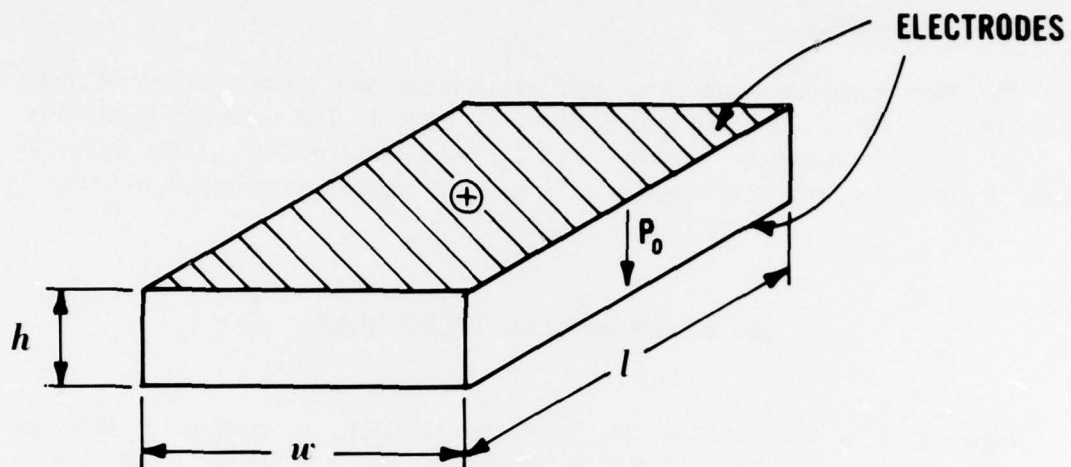


Figure 1. Schematic of PZT element. h is the height, w is the width, and l is the length. During fabrication, electrodes are placed on the top and bottom of the element and it is poled with a large dc voltage through the height to a polarization P_0 . The polarization vector points in the direction from the positive to the negative electrode.

Table 1. Average piezoelectric and ferroelectric properties of PZT elements (Reference 12).

| Material | Dielectric Constant K_3 | Piezoelectric Voltage Coefficient g_{33} ($V \cdot m/N$) | Piezoelectric Charge Coefficient d_{33} (pC/N) | Remanent Polarization P_0 ($\mu C/mm^2$) | Low Frequency Coercive Field E_c (kV/mm) |
|-----------|---------------------------|--|--|--|--|
| PZT 56/44 | 2670 | 18×10^{-3} | 420 | 0.34 | 0.83 |
| PZT 95/5 | 221 | 23×10^{-3} | 45 | 0.30 | 1.0 |

coefficients are useful only for stresses that are not large enough to degrade the piezoelectric properties of the materials. Based on the static depoling data for PZT 56/44 and PZT 95/5, depoling would begin to occur for stresses that are a small fraction of a gigapascal.

The two important parameters that characterize the ferroelectricity of these materials are given in the last two columns of Table I. The remanent polarization P_0 and the low frequency coercive field E_c were obtained for a 60-s hysteresis cycle. E_c is the electric field required to reduce the material polarization to zero.

III. EXPERIMENTAL TECHNIQUES

Figure 2 is a schematic of the experimental setup. It consists of a target assembly containing a PZT unit that is connected with a cable to a high voltage box containing the load capacitor. The impacting projectile depoles the PZT unit thereby releasing the stored surface charge on the electrodes of the unit. The rate of charge release is controlled by the magnitude of the stored surface charge and the shock velocity in the unit. The voltage on the load capacitor is measured with one of the voltage probes shown in Figure 2. The current-viewing resistor measures the released charge to the load capacitor and serves as a check on the voltage measurement.

The PZT unit in the target assembly contained between four and eight stacked PZT elements with a element height of either 3.2 or 6.4 mm. The elements were attached electrically in series with each other with the remanent polarization vector for the unit being directed from the positive to the ground electrode. The PZT unit was depoled in the normal mode since the shock wave propagated in a direction perpendicular to the remanent polarization vector. The unit was encapsulated in a commercially available high-dielectric-strength alumina-filled epoxy (Castall 300-RT7, dielectric breakdown strength 150 kV/mm) to reduce the probability of high voltage electrical breakdown around its edges.

A 40-mm bore diameter gas gun¹³ was used for shock depoling the PZT units. Figure 3 is a schematic of the muzzle region of the gun with a PZT target assembly. The average projectile velocity at impact was measured with the three charged pins in the side of the barrel. The charged trigger pin provided a pulse for triggering the recording oscilloscopes when contacted by the grounded projectile. Disks of quartz, nickel, and 6061-T6 aluminum were used as impactors in these experiments.

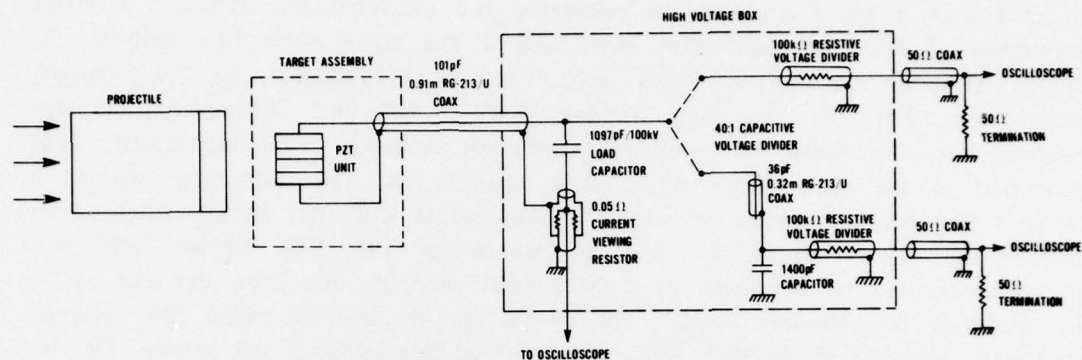


Figure 2. Schematic of experimental arrangement for generating and measuring released charge and voltage from shock-depoled PZT unit. The high voltage box contained either the resistive voltage divider or the combination of capacitive and resistive voltage dividers.

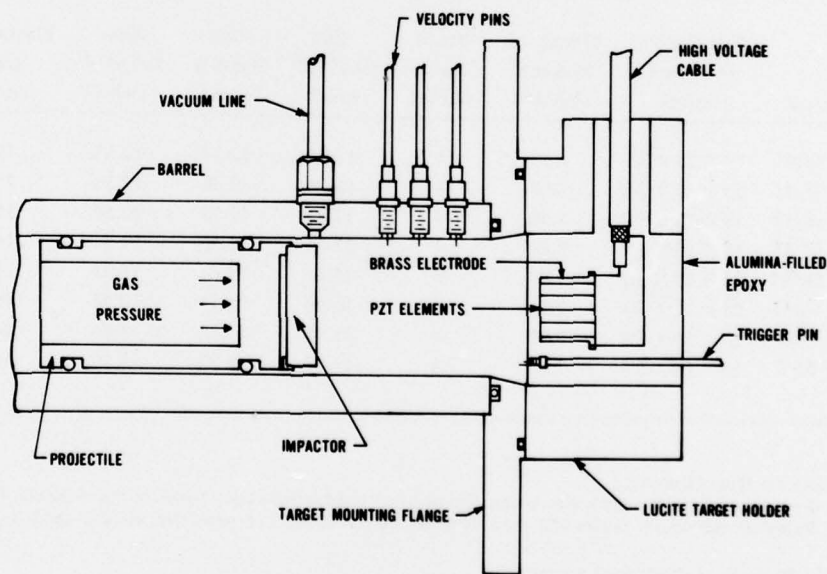


Figure 3. Schematic of muzzle region of gas gun showing the details of the target assembly for normal-voltage-mode depoling of PZT material.

Eight shots were fired: six shots with PZT 56/44 material and two shots with PZT 95/5 material. Table 2 gives the final dimensions of each of the PZT units. Also given are the nominal element size, element density, and number of elements in each unit. Table 3 contains the calculated and measured low frequency electrical properties of the PZT units that were used in the shock wave data analysis. The charge available for release from each unit is proportional to the remanent polarization. The low frequency coercive field is not used directly in the data analysis but is included for comparison with the measured maximum electric fields generated in the units under shock wave compression. The next two columns in Table 3 give the capacitance of each PZT unit before and after epoxy encapsulation, respectively. The decrease in the capacitance of the PZT 56/44 units with encapsulation can be explained as a mechanical clamping effect on the unit by the encapsulating alumina-filled epoxy. The reason for the increase rather than decrease in the capacitance of the PZT 95/5 units with encapsulation is not known. The last column lists the low frequency relative dielectric constant of the units. These values were calculated from the measured capacitances and dimensions of the units. The measured uncertainty in the values listed in this table is estimated to be a few percent.

Table 2. Density and size of PZT elements and units.

| Unit No. | Material | Nominal Size of Element (mm) | Density of Element ^a (Mg/m ³) | No. of Elements in Unit | Unit Height h ^b (mm) | Unit Width w (mm) | Unit Length ℓ^c (mm) | Electroded Area (mm ²) | Unit Volume (cm ³) |
|----------|-----------|------------------------------|--|-------------------------|---------------------------------|-------------------|---------------------------|------------------------------------|--------------------------------|
| 1 | PZT 56/44 | 13 × 13 × 3.2 | 7.58 | 4 | 12.91 | 12.37 | 12.55 | 155 | 2.00 |
| 2 | PZT 56/44 | 13 × 13 × 3.2 | 7.58 | 4 | 12.90 | 12.48 | 12.50 | 156 | 2.01 |
| 3 | PZT 56/44 | 13 × 13 × 3.2 | 7.58 | 4 | 12.89 | 12.53 | 12.50 | 157 | 2.02 |
| 4 | PZT 56/44 | 13 × 13 × 3.2 | 7.58 | 4 | 12.92 | 12.50 | 12.54 | 162 | 2.03 |
| 5 | PZT 56/44 | 25 × 13 × 3.2 | 7.59 | 8 | 25.86 | 25.62 | 12.43 | 311 | 8.04 |
| 6 | PZT 56/44 | 25 × 51 × 6.4 | 7.55 | 4 | 26.09 | 25.15 | 50.24 | 1263 | 32.96 |
| 7 | PZT 95/5 | 25 × 19 × 6.4 | 7.47 | 4 | 25.50 | 24.89 | 18.64 | 464 | 11.83 |
| 8 | PZT 95/5 | 25 × 19 × 6.4 | 7.47 | 5 | 31.99 | 24.22 | 18.50 | 448 | 14.33 |

^aAverage density for three elements.

^bThis height does not include the thickness of the silver-loaded conductive epoxy between the elements. To calculate the unit height including the epoxy layers add 0.15 mm per epoxy layer. The generated electric field is parallel to this direction.

^cParallel to the direction of shock wave propagation.

Table 3. Ferroelectric and dielectric properties of PZT units.

| Unit No. | Remanent Polarization P_0^a ($\mu\text{C}/\text{mm}^2$) | Low Frequency Coercive Field E_C^a (kV/mm) | Capacitance Before Epoxy Encapsulation ^a (pF) | Capacitance After Epoxy Encapsulation ^b (pF) | Relative Dielectric Constant K_3 After Epoxy Encapsulation |
|----------|--|---|---|--|--|
| 1 | 0.33 | 0.86 | 291 | 243 | 2280 |
| 2 | 0.33 | 0.86 | 293 | 239 | 2230 |
| 3 | 0.33 | 0.86 | 293 | 238 | 2210 |
| 4 | 0.33 | 0.86 | 290 | 243 | 2200 |
| 5 | 0.33 | 0.78 | 277 | 238 | 2240 |
| 6 | 0.40 | 0.81 | 1060 | 991 | 2310 |
| 7 | 0.30 | 1.1 | 35 | 43 | 268 |
| 8 | 0.30 | 0.92 | 27 | 38 | 308 |

^aThese values were calculated for each unit from data provided for each element by Gulton Industries, Inc.

^bValues are the average for a frequency between approximately 10 Hz and 10 kHz.

Figure 4 shows a target assembly mounted on the gun muzzle for impacting. The Lucite target holder is 90-mm wide, 102-mm high, and 54-mm deep. The RG-213/U high-voltage cable connecting the PZT unit to the load capacitor extends from the top of the target holder. Figure 5 shows the high voltage box that is located adjacent to the gun muzzle. The box contains the current probe, voltage probe, and load capacitor. The bottom, sides, and 25-mm-wide flange at the top of the box were welded together as a unit from 2.18-mm-thick aluminum sheet. The box is 0.71-m long, 0.31-m wide, and 0.31-m high. The box was filled with clean transformer oil (Exxon Univolt 33, dielectric breakdown strength approximately 3 kV/mm) to prevent high voltage breakdown between the elements in the box. The top of the box is a copper sheet 0.76-m long, 0.36-m wide, and 3.18-mm thick. It was secured to the box at its edges. Panel feed-through connectors (Amphenol UG-30/U) were attached to the top of the box at each end. Some of these connectors were drilled out in the center to permit the passage of the RG-213/U dielectric and center conductor that connected the PZT unit to the load capacitor. All the high voltage components were attached to a Lucite sheet that was suspended from the top of the box with four nylon threaded rods. This arrangement allowed changes to be made inside the box by simply raising the lid.

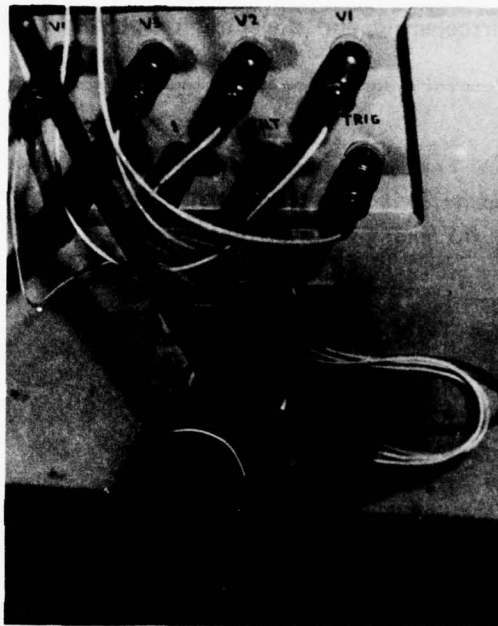


Figure 4. PZT target assembly on gas gun muzzle prior to firing gun.

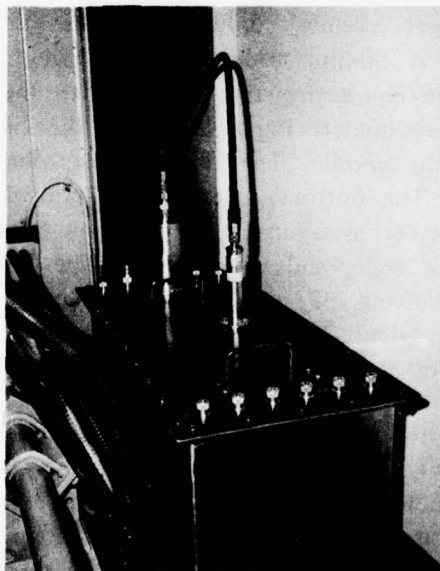


Figure 5. High voltage box showing the resistive voltage probe (at the end of the box) and the current probe (in the middle of the box). This box is located adjacent to the gas gun muzzle.

Figure 6 is a photograph of the high voltage box with the lid raised to show the electrical components. The rectangular item in the middle of the box is the load capacitor. Two different load capacitors were used in these experiments. (High Energy, Inc. Type CP319/409104, 100-kV peak voltage, 1400 ± 5 pF capacitance at 1 kHz and Type CP320/414320, 100-kV peak voltage, 1100 ± 5 pF capacitance at 1 kHz. The capacitors were fixed paper/oil capacitors housed in an inert polypropylene case with dimensions 83 mm \times 89 mm \times 203 mm. In peak voltage tests by the manufacturer, the capacitors were charged to a voltage slightly above 100 kV and held for 2 to 10 s, and then discharged through a 2Ω stainless-steel strap lead.) An average input capacitance of 1097 ± 15 pF for a frequency between 100 Hz and 100 kHz was obtained for the CP 320 capacitor after it was placed in the high voltage box. In one of the shots a high voltage diode was placed in the high voltage side of the electrical circuit between the PZT unit and load capacitor. This was done to determine how effectively the charged load capacitor could be isolated from the depoled PZT unit which may become shorted after the passage of the shock wave. In the shots without a diode, during or after the passage of the shock wave through the units, the large generated electric fields along with shock and relief wave conditions caused the load voltage to decrease. The high voltage diode (Semtech Corporation High Voltage, High Current Silicon Rectifier, Part No. SA5608, 250-ns recovery time, 100-kV peak inverse voltage, 1-pF capacitance, 222-mm long \times 25-mm diameter) can be seen to the left of the load capacitor in Figure 6. Also shown are corona balls at the ends of the electrical elements for minimizing high voltage corona discharge from the sharp metal screw threads.

Three different resistive voltage dividers (T&M Research Products, Inc.) were used in the experiments to measure the load voltage. Each divider had a division ratio of approximately 2000 to 1, an input impedance of 50Ω , and a voltage risetime less than 25 ns. Probes 1 and 2 had a maximum input voltage of 50 kV and Probe 4 had a maximum input voltage of 100 kV. A probe consists basically of a high resistance center conductor (100 k Ω resistance made by a special winding of carbon resistors) inside a coaxial ground case. Two small capacitors in the picofarad range (one variable and one fixed) are connected from the center conductor to the ground case. The division ratio occurs when a 50Ω coaxial cable and 50Ω termination resistor are connected to the probe output as indicated in Figure 2.¹⁴

The probes were calibrated under pulsed high voltage conditions at the National Bureau of Standards.¹⁵ The high voltage calibration pulse had a nominal risetime of 1 μ s to a constant amplitude region having a nominal duration of 6 μ s. This input pulse is similar to that in an actual PZT depoling experiment. The test results are

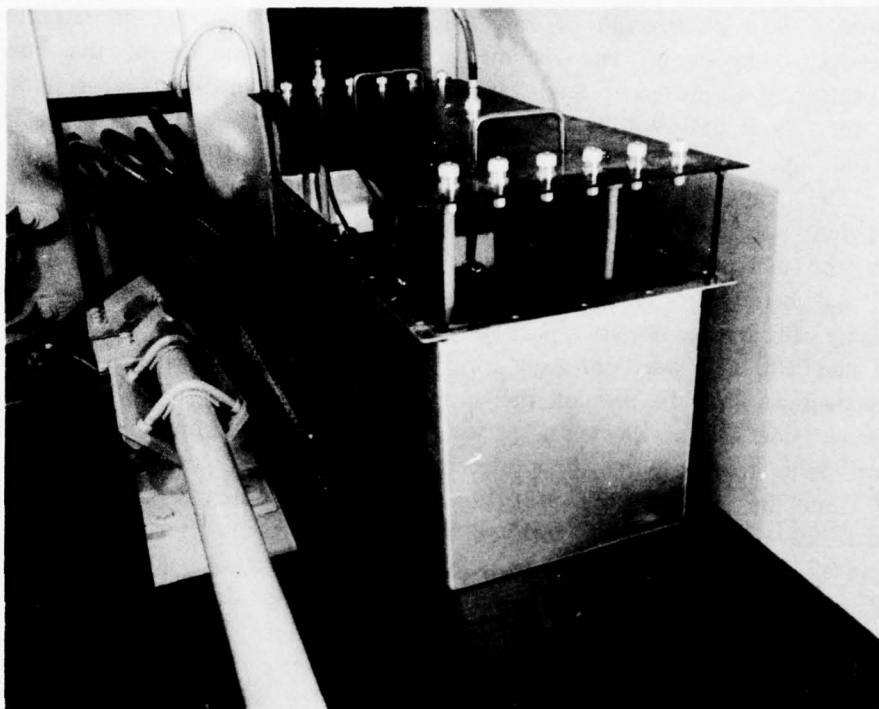


Figure 6. High voltage box with the lid raised showing the electrical components in the box.

listed in Table 4. The uncertainty in the division ratio was estimated to be less than $\pm 10\%$ for the nominal input voltage of 10 kV and to be less than $\pm 5\%$ for the other listed input voltages. Voltage calibration curves of output voltage versus input voltage were constructed from this table and used in the experimental data analysis.

A resistive voltage divider was used directly to measure the load voltage for the first five shots of the series. For the last three shots of the series a capacitive voltage divider was constructed and used in conjunction with Probe 2. The electrical schematic of this combination probe is shown in Figure 2. A division ratio of 74,200 to 1 was measured for this combination probe under low voltage conditions. This measured value compares favorably with a calculated value of 73,200 to 1. (The calculated division ratio was obtained by multiplying the calculated capacitive divider ratio (40 to 1) and the measured 10-kV division ratio for Probe 2 in Table 4.)

**Table 4. National Bureau of Standards calibration results
for T&M resistive voltage probes.**

| Probe No. | Input Voltage (kV) | Division Ratio |
|--------------|--------------------------|-------------------|
| 1 | 10 | 1920 |
| | 27 | 1880 |
| | 32 | 1860 |
| | 39 | 1820 |
| 2 | 10 | 1830 |
| | 23 | 1840 |
| | 33 | 1750 |
| | 35 | 1750 |
| 4 | 10 | 1790 |
| | 27 | 1800 |
| | 41 | 1760 |
| | 63 | 1750 |
| | 77 | 1680 |

The coaxial current-viewing resistors (T&M Research Products, Inc.) used for measuring the circuit current had a nominal resistance of 0.05Ω , a bandpass frequency greater than 300 MHz, and a maximum energy rating greater than 20 J. A summary of the voltage and current probes used for each shot is given in Table 5. For the current probes the value of the actual resistance is also reported. Table 6 lists the projectile and target impact parameters. The PZT units in the target assemblies were completely encapsulated with the alumina-filled epoxy. The distance from the epoxy impact surface of the target assembly to the PZT material (see Figure 3) is also given in this table. The projectile impact velocity is the average velocity for two or three velocity intervals and has an estimated uncertainty of about 0.5%.

Zero stress longitudinal and shear wave velocity measurements were made on the PZT ceramics for comparison with the shock data. Dapco longitudinal and shear velocity transducers were used for the measurements. The transducers were used with a Panametrics Model 5050 PR ultrasonic pulser/receiver. Dapco couplant paste was

Table 5. Voltage and current probes used for each shot.

| Shot No. | Voltage Probe | Current Probe |
|----------|---------------|-------------------------------|
| 71 | 1 | None |
| 83 | 4 | SBNC-2-05 0.05118 Ω |
| 84 | 4 | 2M05 0.05130 Ω |
| 85 | 4 | 2M05 0.05130 Ω |
| 87 | 4 | 2M05 0.05130 Ω |
| 121 | Combination | SBNC-1-05 0.04916 Ω |
| 122 | Combination | SBNC-1-05 0.04916 Ω |
| 123 | Combination | SBNC-1-05 0.04916 Ω |

used to couple the transducers to the specimens. The time between the echos was measured using a Tektronix R7704 oscilloscope with a 7D11 digital delay plug-in unit. The uncertainty in these measurements is about 1% or less.

Table 6. Projectile and target impact parameters.

| Shot No. | PZT Target Assembly No. | Impactor Material | Impactor Thickness (mm) | Impactor Diameter (mm) | Distance of PZT Unit From Impact Surface of Target Assembly (mm) | Impactor Velocity (km/s) |
|----------|-------------------------|---------------------|-------------------------|------------------------|--|--------------------------|
| 71 | 1 | Quartz ^a | 6.37 | 35.6 | 3.97 | 0.558 |
| 83 | 2 | Quartz | 6.35 | 35.6 | 3.48 | 0.772 |
| 84 | 3 | Quartz | 6.35 | 35.6 | 3.35 | 0.908 |
| 85 | 4 | Nickel ^b | 6.35 | 35.6 | 3.36 | 0.968 |
| 87 | 5 | 6061-T6 Al | 9.53 | 35.6 | 3.43 | 0.916 |
| 121 | 6 | 6061-T6 Al | 12.7 | 35.6 | 3.44 | 0.917 |
| 122 | 7 | 6061-T6 Al | 12.7 | 35.6 | 4.23 | 0.353 |
| 123 | 8 | 6061-T6 Al | 9.53 | 40.0 | 4.24 | 0.178 |

^aThe quartz impactors were X-cut with approximately 25 kÅ of chrome/gold deposited on their entire surface. They were purchased from Valpey-Fisher Corporation.

^b98 wt. % pure nickel, hardness R_b 43.

IV. PZT TARGET ASSEMBLY FABRICATION

This section contains a detailed description of the PZT target assembly fabrication technique. The first step in the procedure is the careful selection and preparation of the ferroelectric ceramic elements. Each element must be free of chipped corners and edges. A chipped region will tend to fill with conductive epoxy when the elements are assembled into a unit; these regions may serve as electrical stress concentrators and potential dielectric breakdown sites. Figure 7 shows two brass electrodes and four PZT ferroelectric elements prior to assembly.

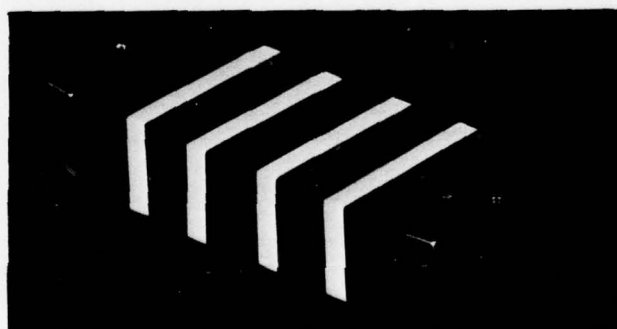


Figure 7. PZT elements and brass electrodes prior to assembly into a unit.

Stranded copper wires (AWG 14) are soldered to each brass electrode and the positive electrode is engraved with a plus sign. The brass pieces are lightly lapped with #1 Buehler emery paper and then cleaned with acetone. The electrode surfaces of each ceramic element are lightly lapped with #4/0 Buehler emery paper and wiped with an acetone-saturated Kimwipe. The dimensions of each element and the brass electrodes are then measured with a micrometer. A two-part, room-temperature-cure, silver-loaded conductive epoxy paste (Dynaloy 326) is spread over each electrode surface and (observing polarities) the parts of the unit are carefully wrung together to ensure uniform epoxy coverage. The assembled unit is then placed in a hinged-beam clamp as shown in Figure 8. The large rectangular beam has V-grooves in its underside at two opposite edges. Brass rods (3.2-mm diameter) fit into these grooves. One rod rests in a groove in a supporting rail to form a hinge and the other rod rests on the ferroelectric unit. This arrangement provides vertical loading of the unit while minimizing shear motion. The parts of the clamp are coated with fluorocarbon dry release agent. Final alignment is accomplished by pressing the end of a machinist's scale against the sides of the unit. After the epoxy has cured, the unit is loosened from the clamp by gently tapping a razor blade edge between the unit and the parts of the clamp.

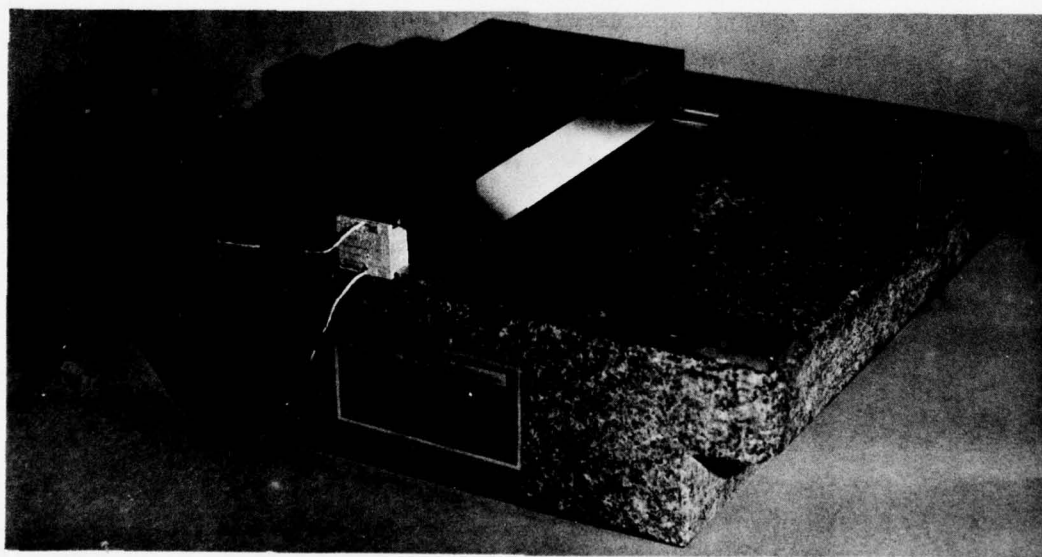


Figure 8. PZT unit compressively held in a hinged-beam clamp during conductive epoxy cure.

An assembled unit is shown in Figure 9. The excess conductive epoxy has been removed by carefully lapping the sides of the unit with #1 Buehler emery paper on a granite surface plate. The region between the wires is lapped with emery paper on a granite parallel. In the final stages of excess epoxy removal, it is important to lap parallel to the epoxy seams between the ceramic elements to minimize the embedding of conductive material into the ceramic surfaces.

During and after assembly, all handling of the unit is done with polyethylene gloves. This is to prevent contamination of the ceramic surfaces by moisture or oil from the skin. Surface contamination can degrade the adhesion of the high voltage potting compound and may provide sites for electrical breakdown. The dimensions of the completed unit are then measured with a micrometer. Capacitance bridge measurements (General Radio Type 716C) are performed on each unit over the frequency range 10 Hz to 10 kHz. Completed units are then stored in a desiccator to minimize the buildup of a moisture layer on the exposed ceramic surfaces, pending assembly into target configurations.

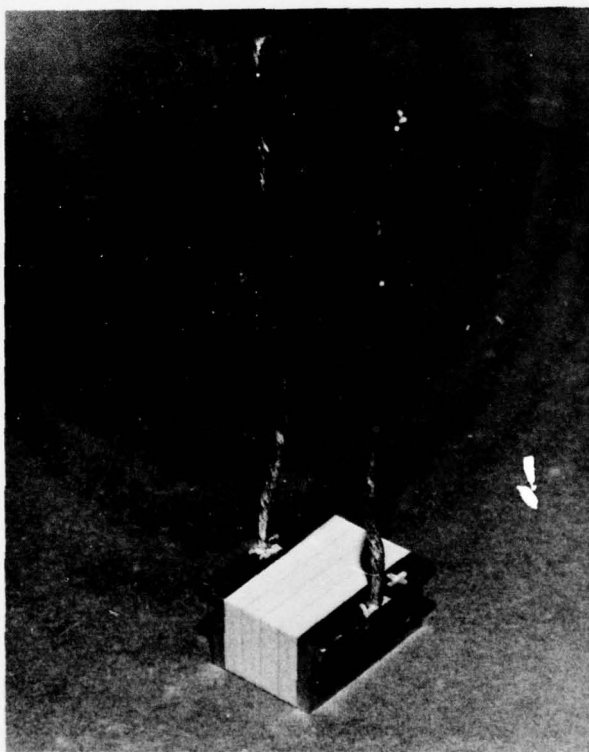


Figure 9. Completed PZT unit.

A Lucite holder was designed to facilitate the uniform assembly of ferroelectric units into target configurations and the mounting of these configurations on the muzzle of the gas gun. A series of brass fixtures was designed to permit the reproducible positioning of units of different dimensions in the Lucite holders during initial potting. Figure 10 shows a unit clamped on a brass fixture. The fixture also facilitates the positioning of an instrumentation trigger pin (a modified 50- Ω printed circuit board connector, Microdot Leptra-Con Part No. 141-0004-0001) shown adjacent to the unit. Those parts of the fixture that are exposed to possible contact with the potting compound are coated with fluorocarbon dry release agent.

In Figure 11 the fixture and ceramic unit have been inserted into a Lucite holder. The distance from the impact plane of the holder to the surface of the unit is being measured with a dial indicator. The parallelism of the impact plane of the holder and the corresponding plane of the PZT unit is maintained to less than 5 mrad. Measurements are taken at four equispaced positions on the holder surface and also on the four corners of the unit (the dial indicator tip touches only the brass electrodes, not the ceramic). It is important to know the thickness of the potting compound that will fill the region between the impact plane and the surface of the unit. Shock wave propagation times and associated time delays can then be estimated for setting the oscilloscopes for pulse diagnostics.

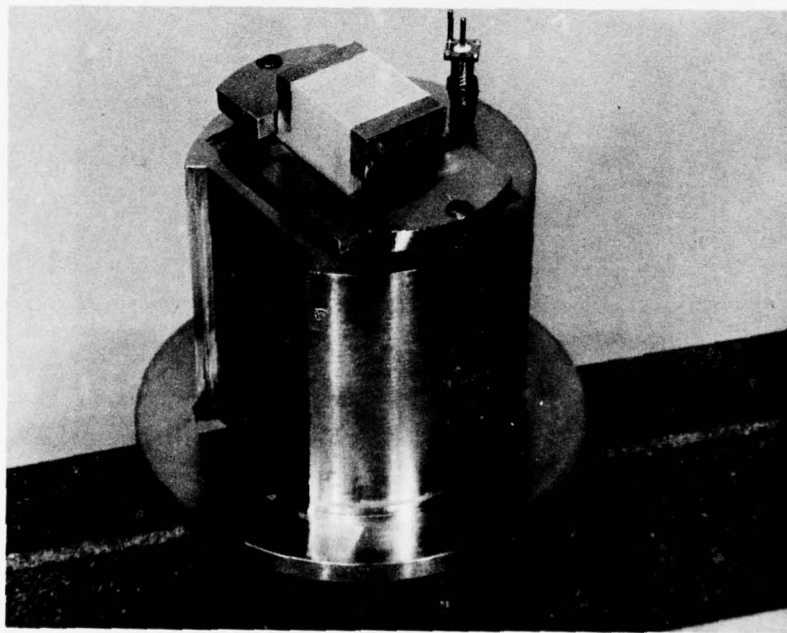


Figure 10. PZT unit and trigger pin positioned on brass fixture prior to insertion into Lucite target holder.

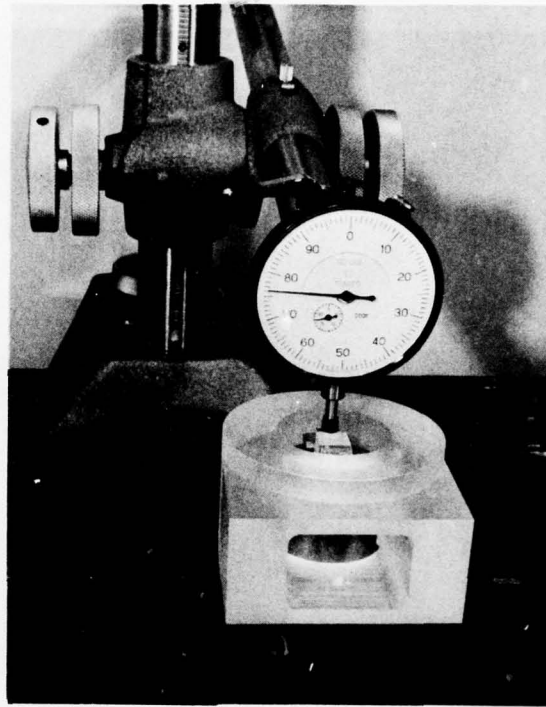


Figure 11. Experimental arrangement for measuring the distance between the impact plane of the target assembly and the PZT unit.

Figure 12 shows the target holder and unit alignment fixture inverted on a granite surface plate, ready for the initial injection of potting compound. The wires from the unit protrude from a slot in the brass fixture. The rod to the right of the wires is attached to the trigger pin. The threaded pin is screwed into a nut that is soldered to the lower end of the rod. The exposed threads and the nut are wrapped with teflon tape to prevent adherence of the potting compound and to provide a clearance cavity in the cured compound for attaching a coaxial cable connector. The rod is free to move vertically so that the tips of the pin rest on the granite gauging surface (and hence in the plane of impact loading) during potting. The rod and pin are also rotationally aligned with fiducial marks to ensure the maximum spacing between the pin and the unit. Prior to potting, the granite surface plate is coated with a thin film of dry release agent. A slot in the left side of the brass fixture facilitates injection and vacuum degassing of the potting material. A large toroidal weight is added to the fixture to ensure good sealing contact between the Lucite holder and the granite surface.

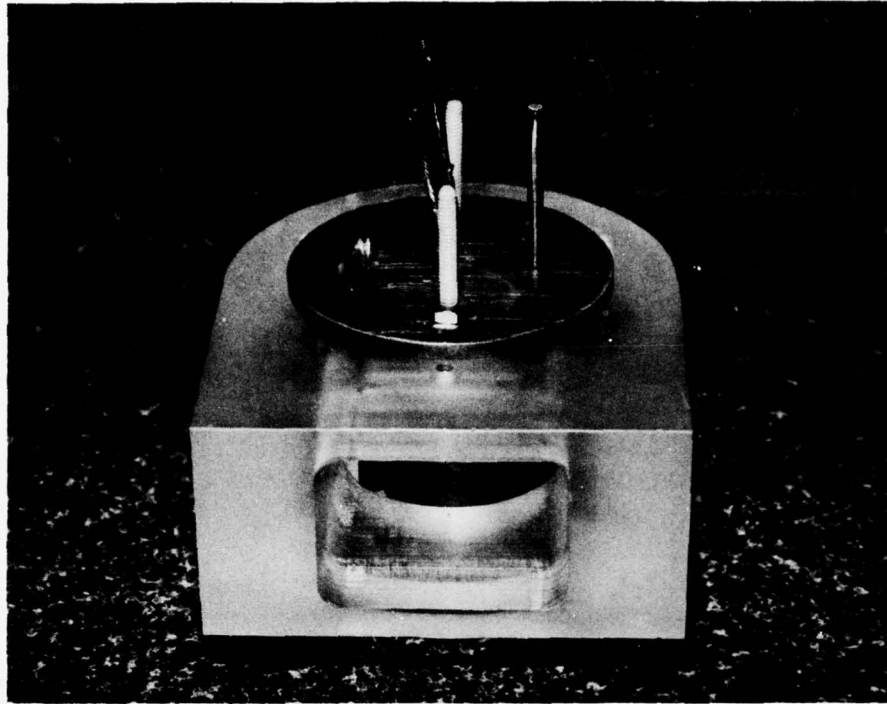


Figure 12. Target holder with brass fixture containing PZT unit and trigger pin on granite surface plate prior to first epoxy pour.

Vacuum degassed (1 Pa, 10 min) alumina-filled epoxy is injected until the level has risen to about 4 mm onto the unit. The granite surface plate and target assembly items are then covered with a bell jar for additional vacuum processing (1 Pa, 10 min) to remove any trapped air resulting from the injection of the potting compound. The pressure is then returned to atmospheric for a 24-hr curing period.

Figure 13 shows a target assembly after the initial potting and the removal of the fixture. The teflon tape has been removed from around the trigger pin and a 50- Ω coaxial cable (RG-188/U) has been attached. A second vacuum potting is then performed which results in the total encapsulation of the unit. After this potting the RG-213/U output cable is then attached to the PZT unit. The cable dielectric is exposed about 20 mm and the center conductor is connected to the positive electrode of the unit. The outer conductor braid is connected to the stranded wire from the negative electrode. The braid is drawn back over the cable jacket and the stranded wire is crimped to the braid with a ferrule (from an AMP Part No. 51692-2 connector). The exposed conductors are then insulated by filling the

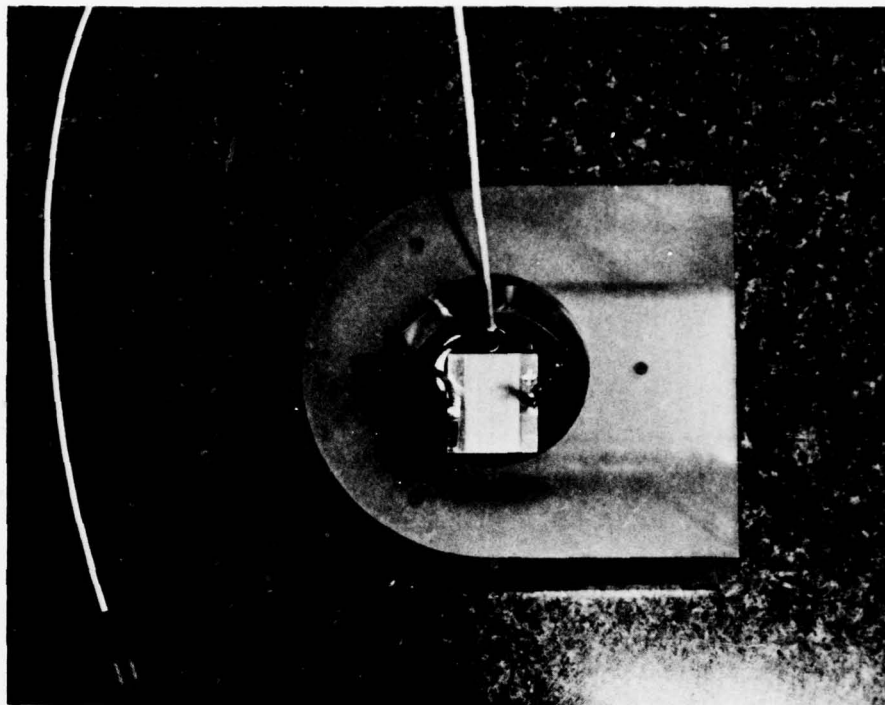


Figure 13. Target assembly showing PZT unit and attached trigger pin cable after first epoxy pour and removal of brass fixture.

remaining volume of the Lucite holder with a silicone high voltage potting compound (Dow Corning Sylgard 110) or with more Castall 300 epoxy. After all the potting material has cured, the target assembly is removed from the granite surface plate by gently tapping a razor blade edge under the side of the holder. The impact surface is then lightly lapped with #2/0 Buehler emery paper on a granite surface plate. This is to remove any excess potting compound that may have seeped under the holder during initial potting.

Figure 14 shows the impact surface of a completed target assembly. The tips of the two conductors of the trigger pin are seen exposed in the impact plane. One of these conductors will be charged to -50 V by the velocity pin charging circuit for the gas gun. The other conductor is grounded. The conducting surface of the impactor disk provides a shorting path across the tips, resulting in the generation of a trigger signal. Prior to mounting the target assembly on the gas gun muzzle, a bead of indium solder is applied to each tip. The height of each bead from the

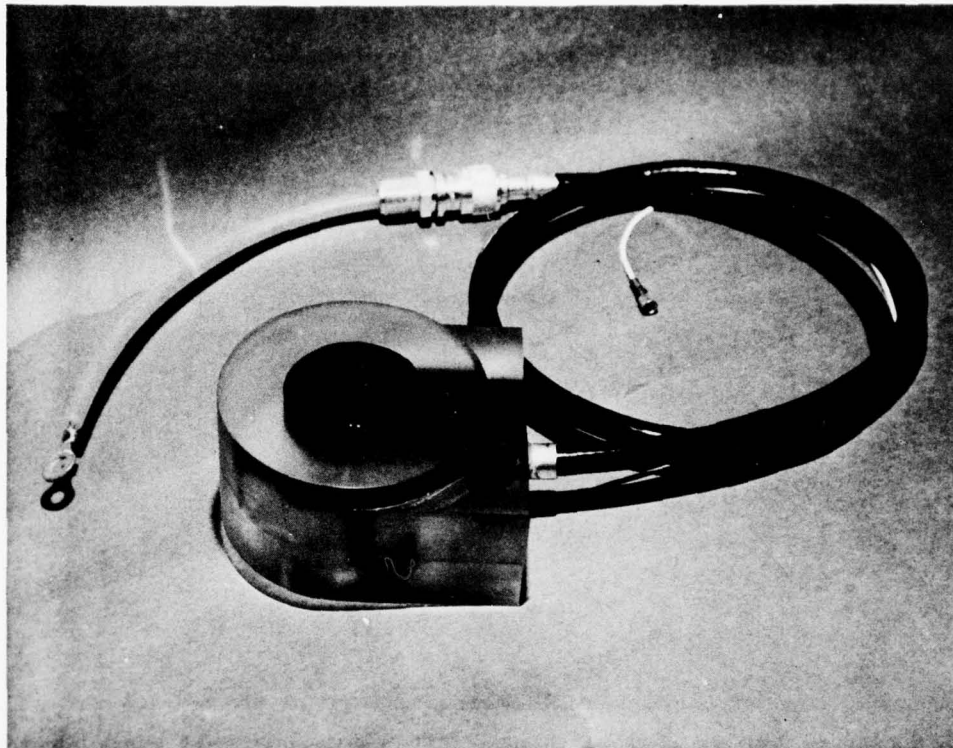


Figure 14. Completed PZT target assembly.

impact plane is adjusted by flattening the indium with the probe of a vernier height gauge while the assembly is supported with granite parallels on a granite surface plate. The grounded conductor bead and the charged conductor bead are adjusted to extend approximately 0.6 mm and 0.5 mm, respectively, from the impact plane of the target assembly. This procedure ensures that the impactor disk will contact the grounded conductor prior to contacting the charged conductor for reliable operation of the trigger circuit.

The braidless portion of RG-213/U cable is for connection of the PZT unit to the load capacitor in the oil-filled box. A connector (AMP Part No. 51692-2), drilled out to permit passage of the RG-213/U center conductor and dielectric, is then crimped onto the cable. A drilled-out panel feedthrough connector is shown screwed onto the cable connector (Figure 14). This type of cable termination has been tested under oil to 100 kV dc without dielectric breakdown.

V. SIMPLIFIED MODEL

The electrical response of a shock-compressed ferroelectric ceramic is a complicated phenomenon and to date a detailed theory has not been developed.⁴ Since the development of a detailed theory is not within the scope of this report only a simplified model will be presented for the normal-mode shock-depoling of a PZT unit with a capacitive load. The model will be used only as a guide in interpreting the experimental data.

A schematic of the shock depoling of a PZT unit is given in Figure 15. The electric displacement vector, electric field, polarization vector, and permittivity are given by $D(t)$, $E(t)$, $P(t)$, and ϵ , respectively. A steady shock wave is assumed for this model. As the shock wave passes through the PZT unit the remanent polarization vector P_0 is reduced in magnitude behind the shock front. For complete depoling, P_0 is reduced to zero. The electric fields $E_1(t)$ and $E_2(t)$ are equal in magnitude and increase with time. If the permittivities ϵ_1 and ϵ_2 are not equal, then the released surface charge densities σ_1 and σ_2 behind and ahead of the shock front, respectively, are related through the equation $\sigma_1/\sigma_2 = \epsilon_1/\epsilon_2$. For example, if the permittivity decreases under shock wave compression then the charge per unit area will be less behind the shock front than ahead of the shock front. For this case, the equivalent capacitance of the PZT unit would decrease as the shock wave passed through it. In this simplified model it will be assumed that the permittivity of the PZT material is constant. It will also be assumed that no electrical breakdown or conduction occurs in the unit and that after the PZT unit comes under shock wave compression it remains in that stress state.

At time t , as the shock wave propagates through the PZT unit, the capacitances behind and ahead of the shock front are given, respectively, by

$$C_1(t) = \frac{wUt}{h} \epsilon, \quad 0 \leq t \leq \tau, \quad (1)$$

and

$$C_2(t) = \frac{w(\ell - Ut)}{h} \epsilon, \quad 0 \leq t \leq \tau, \quad (2)$$

where $\tau = \ell/U$ is the shock transit time through the PZT unit and $\epsilon = \epsilon_1 = \epsilon_2$. The equivalent capacitance of the PZT unit is constant and given by

$$C = C_1(t) + C_2(t) = \frac{A}{h} \epsilon, \quad t \geq 0, \quad (3)$$

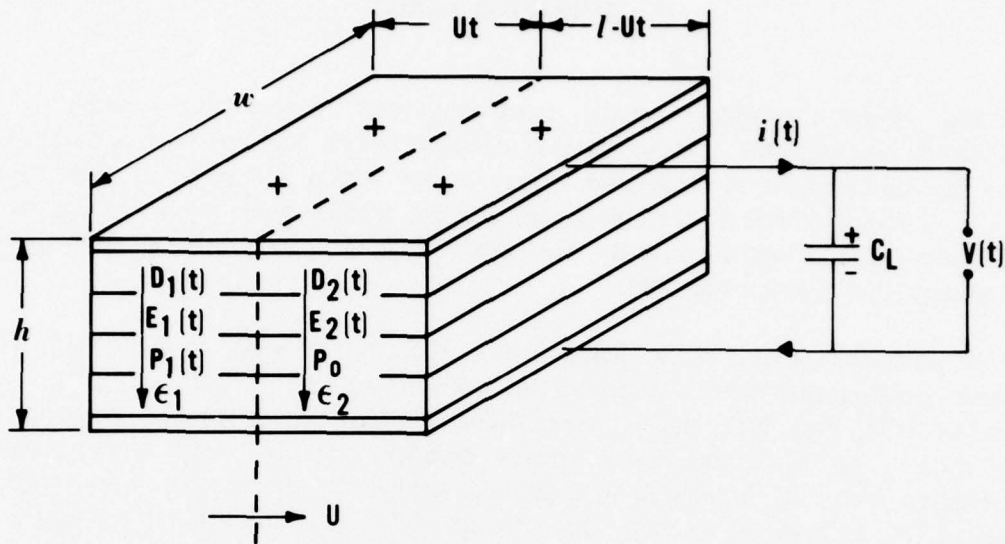


Figure 15. Schematic of the normal-voltage-mode depoling of a PZT unit with a capacitive load. U is the shock velocity. At time t the shock front is indicated by the dashed line. Regions 1 and 2 are behind and ahead of the shock front, respectively. As the shock wave passes through and depoles the unit, bound surface charge behind the shock front is released. This released charge is distributed between the PZT unit and load capacitance C_L , charging them to a voltage $V(t)$.

where $A = \ell w$. In this analysis the strain behind the shock front is considered to be negligible. The charge conservation equation is

$$Q(t) = q(t) + q_L(t), \quad t \geq 0, \quad (4)$$

where $Q(t)$ is the charge released by the shock wave and $q(t)$ and $q_L(t)$ are the charges distributed on the source and load capacitances, respectively. The voltage balance equation is

$$\frac{q(t)}{C} = \frac{q_L(t)}{C_L}, \quad t \geq 0, \quad (5)$$

From Equations (4) and (5)

$$q(t) = \frac{C}{C+C_L} Q(t), \quad t \geq 0, \quad (6)$$

and

$$q_L(t) = \frac{C_L}{C+C_L} Q(t), \quad t \geq 0, \quad (7)$$

where $C+C_L$ is the circuit capacitance. The voltage on the PZT unit and load capacitance is then given by

$$V(t) = \frac{Q(t)}{C+C_L}, \quad t \geq 0. \quad (8)$$

The current flowing to the load capacitor is

$$i(t) = \frac{dq_L(t)}{dt} = \frac{C_L}{C+C_L} \frac{dQ(t)}{dt}, \quad t \geq 0. \quad (9)$$

If it is assumed that the shock wave releases all the bound surface charge instantaneously on compression, then the released charge is

$$Q(t) = \begin{cases} P_0 A \frac{t}{\tau}, & 0 \leq t \leq \tau, \\ P_0 A, & t > \tau. \end{cases} \quad (10)$$

The equations for $V(t)$ and $i(t)$ then become, respectively,

$$V(t) = \begin{cases} \frac{P_0 A}{C+C_L} \frac{t}{\tau}, & 0 \leq t \leq \tau, \\ \frac{P_0 A}{C+C_L}, & t > \tau. \end{cases} \quad (11)$$

and

$$i(t) = \begin{cases} \frac{C_L}{C+C_L} \frac{P_0 A}{\tau}, & 0 \leq t \leq \tau, \\ 0 & , t > \tau. \end{cases} \quad (12)$$

These equations are plotted in Figure 16(a). This type of response for a PZT unit will be called ideal. The voltage and current pulses for one of the PZT 95/5 shots showed this type of behavior.

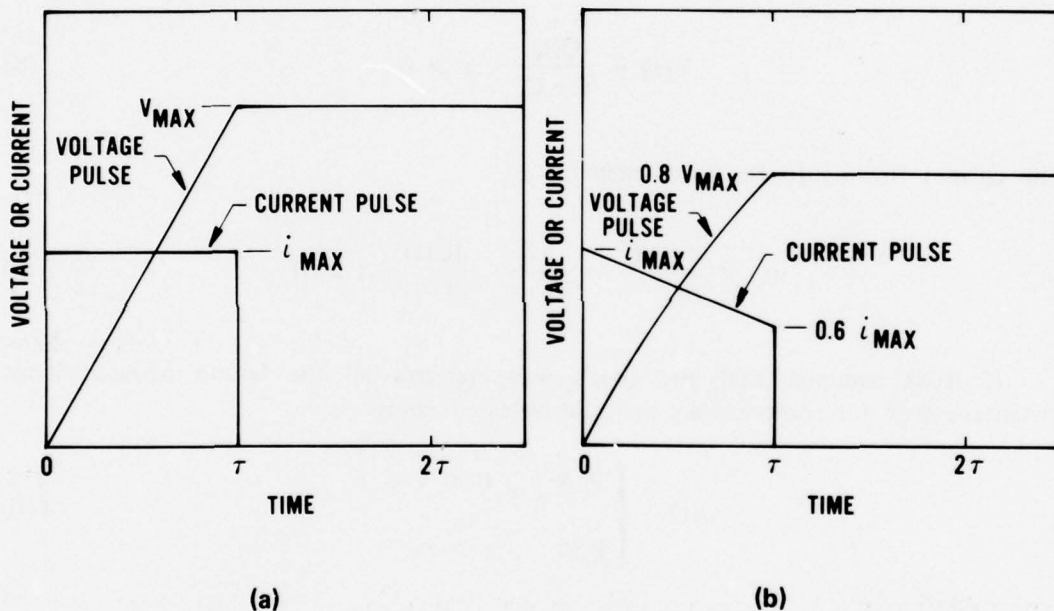


Figure 16. Schematic of voltage and current pulses for the normal mode depoling of a PZT unit. (a) Pulses for the ideal response of a PZT unit. The voltage pulse increased linearly to maximum value of $V_{max} = (P_0 A)/(C + C_L)$. The current pulse has a constant maximum value of $i_{max} = (C_L/(C + C_L))(P_0 A/\tau)$ during shock transit time τ . (b) Pulses for the nonideal response of a PZT unit. For $\alpha = 0.2 P_0/\tau$ the voltage pulse increases in a nonlinear manner to a maximum value of $0.8 V_{max}$. The current pulse decreases linearly from i_{max} to $0.6 i_{max}$ during shock transit time.

In most of the experiments the PZT units did not respond in an ideal manner since the charge flowing from the units decreased in time as the shock wave propagated through them. Although the reason for the decreased charge flow probably depends in a complicated manner on the shock conditions and the PZT material properties, this behavior can be represented in simple terms by the expression

$$Q(t) = \begin{cases} P_0 A \frac{t}{\tau} \left(1 - \frac{\alpha t}{P_0}\right), & 0 \leq t \leq \tau, \\ P_0 A \left(1 - \frac{\alpha \tau}{P_0}\right), & t > \tau. \end{cases} \quad (13)$$

In Equation (13) a linear decrease in the charge release has been assumed. The constant parameter α has the dimensions (charge area⁻¹ time⁻¹). For those shots in which depoling is initially incomplete, P_0 could be replaced by a smaller value.

Substituting Equation (13) into Equations (8) and (9) gives, respectively,

$$V(t) = \begin{cases} \frac{P_0 A}{C + C_L} \frac{t}{\tau} \left(1 - \frac{\alpha t}{P_0}\right), & 0 \leq t \leq \tau, \\ \frac{P_0 A}{C + C_L} \left(1 - \frac{\alpha \tau}{P_0}\right), & t > \tau. \end{cases} \quad (14)$$

and

$$i(t) = \begin{cases} \frac{C_L}{C + C_L} \frac{P_0 A}{\tau} \left(1 - 2 \frac{\alpha t}{P_0}\right), & 0 \leq t \leq \tau, \\ 0, & t > \tau. \end{cases} \quad (15)$$

These equations are plotted in Figure 16(b) for a representative α of $0.2 P_0/\tau$. For this value of α , $Q(\tau) = 0.8 P_0 A$, that is, the charge release is 80%. Note that the slopes of the voltage pulses for the ideal and nonideal responses are equal at $t = 0$. The value α can be determined from the decrease in the current pulse amplitude with the equation

$$\alpha = \frac{P_0}{2\tau} \left(\frac{i_{\max} - i(\tau)}{i_{\max}} \right), \quad (16)$$

where $i(\tau)$ is the value of the current at $t = \tau$.

The equations for the charge release, voltage, and current that have been derived for the ideal and nonideal responses of PZT units depend on the ratio of the load to source capacitances, C_L/C . Appendix A contains a discussion of these equations as a function of this ratio for the ideal response of a PZT unit.

VI. RESULTS AND DISCUSSION

Table 7 is a summary of the voltage measurements. The input shock stress for the PZT units was calculated using the measured impactor velocities in Table 6, the known Hugoniot equations of state for the impactor materials quartz,¹⁶ nickel,¹⁷ and 6061-T6 aluminum,¹⁸ and the Hugoniot for the target assembly materials. The Hugoniot for the PZT encapsulating material, Castall 300, has been previously determined.¹⁹ Since the Hugoniot of the PZT 56/44 material has not been measured, the Hugoniot of PZT 52/48²⁰ (density 7.58 Mg/m^3) was used in the calculations. (PZT 52/48 is a solid solution containing 52 mole % lead zirconate and 58 mole % lead titanate with niobium as a minor added constituent.) For the PZT 95/5 material the Hugoniot of normally sintered PZT 95/5³ (density 7.72 Mg/m^3) was used.

Voltage and current outputs are presented in Figures 17 through 24. The current outputs include the charge transferred to the 0.91-m RG-213/U cable and, where appropriate, to the capacitive voltage divider. The transit time for the depoling stress wave is indicated by the dashed line on the time axis in the figures. Appendix B contains the records from which these outputs were obtained. The high frequency ringing that occurred on the initial part of some of the current records was removed by averaging the amplitude of the high frequency oscillations during the pulse digitization procedure.

Electrical breakdown occurred in five shots. In Shots 85, 121, 122, and 123 breakdown occurred before the depoling stress wave had propagated through the PZT unit; in Shot 87 breakdown occurred after the depoling wave had propagated through the unit. It is not known whether the stress-induced electrical breakdown is a bulk phenomenon occurring uniformly within the PZT unit or whether it is occurring nonuniformly along electrical short circuit paths within the material or at the PZT - epoxy interface. The voltage pulses showed an abrupt decrease in amplitude at breakdown in four of the shots whereas in Shot 85 the voltage decrease at breakdown was less abrupt. In Shots 85, 121, and 122 recovery pulses were observed after electrical breakdown. A recovery pulse was not observed in Shot

Table 7. Summary of voltage measurements for shock-depoled PZT units.

| Shot No. | Material | Charge Available for Release (μC) | Calculated | | Maximum Load Voltage (kV) | Time to Maximum Voltage (μs) | Maximum Electric Field in PZT Unit (kV/mm) | Velocity of Depoling Stress Wave ^b (km/s) | Initial Slope of Voltage Pulse (kV/ μs) | Maximum Load Energy ^c (J) | Maximum Load Energy Density ^d (J/cm ³) | Average Power Transferred to Load ^e (kW) |
|----------|-----------|--|---------------------------------|--|------------------------------------|---|--|--|---|--------------------------------------|---|---|
| | | | Input Stress for PZT Unit (GPa) | Total Load Capacitance ^a (pF) | | | | | | | | |
| 71 | PZT 56/44 | 51 | 4.4 | 1501 | 19 | 2.88 | 1.5 | 4.36 | 8.7 | 0.27 | 0.14 | 93 |
| 83 | PZT 56/44 | 51 | 6.4 | 1198 | 25 ^f | 2.51 ^j | 1.9 | 4.99 | 11 | 0.37 | 0.18 | 150 |
| 84 | PZT 56/44 | 51 | 7.8 | 1198 | 27 ^f | 2.60 ^j | 2.1 | 4.80 | 14 | 0.45 | 0.22 | 170 |
| 85 | PZT 56/44 | 53 | 11.8 | 1198 | 12 ^g 5 ^h | 0.79 ^g 2.93 ^h | 0.93 0.39 | — 4.28 | 17 — | 0.086 — | 0.042 — | 110 ^l — |
| 87 | PZT 56/44 | 102 | 7.9 | 1198 | 55 | 2.57 | 2.1 | 4.84 | 36 | 1.8 | 0.22 | 710 |
| 121 | PZT 56/44 | 508 | 7.9 | 1233 | 45 ^g 26 ^h | 5.25 ^g 14.7 ^h | 1.7 1.0 | — 3.42 ^k | 20 — | 1.3 — | 0.039 — | 240 ^l — |
| 122 | PZT 95/5 | 140 | 2.9 | 1233 | 81 ^g 6 ^h | 3.58 ^g 4.74 ^h | 3.2 0.23 | — 3.93 | 24 — | 4.1 — | 0.35 — | 1100 ^l — |
| 123 | PZT 95/5 | 136 | 1.4 | 1233 | 64 ^{g,i} | 4.27 ^{g,i} | 2.0 | 4.33 | 17 | 2.5 | 0.17 | 590 ^l |

^aValues are the average for a frequency between 100 Hz and 100 kHz. The total load capacitance includes the capacitance of the 0.91-m RG-213/U cable and, where appropriate, the capacitive voltage divider.

^bCalculated using length of PZT unit and time to maximum voltage, or in the case of electrical breakdown, the time to maximum voltage for the recovered pulse.

^cObtained from the formula $0.5 C_L V^2$ where C_L is the load capacitance and V is the maximum load voltage.

^dMaximum load energy per cm³ of PZT material.

^eThe average power or rate at which energy is transferred to the load was obtained by dividing the maximum load energy by the time to maximum voltage.

^fExtrapolated voltage at a time corresponding to an abrupt decrease in the current pulse amplitude.

^gVoltage and time just before electrical breakdown.

^hV value for recovery pulse.

ⁱThere was no recovery pulse for this shot. The voltage fell to zero at 4.97 μs ; if this time is used a depoling stress wave velocity of 3.72 km/s is obtained.

^jTime corresponding to an abrupt decrease in the current pulse amplitude.

^kThis value is low compared with the depoling stress wave velocity for the five preceding PZT 56/44 shots indicating that the time to maximum voltage is longer than expected. The reason may be that the unit experienced shock and relief wave interactions over most of the time duration of the depoling stress wave causing complicated electrical relaxation phenomena to occur. The average velocity for the five preceding shots was 4.65 km/s giving 10.8 μs for the calculated transit time for this shot.

^lValues calculated using the time before electrical breakdown occurred in the PZT target assembly.

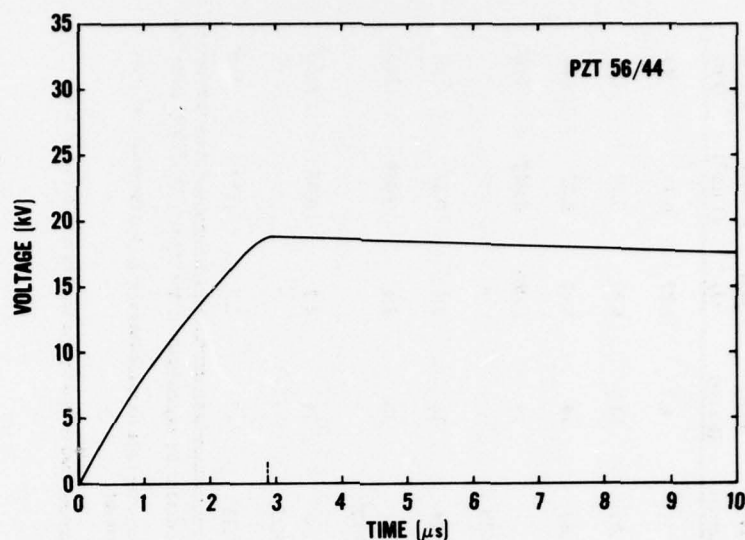


Figure 17. Voltage pulse for PZT 56/44 unit in Shot 71. The load capacitance was 1501 pF and the input shock stress was 4.4 GPa. For this shot a high voltage diode was placed between the PZT unit and load capacitor. After a peak voltage was achieved at 2.88 μ s the voltage slowly decayed with the 130- μ s time constant of the load capacitor – resistive voltage divider system.

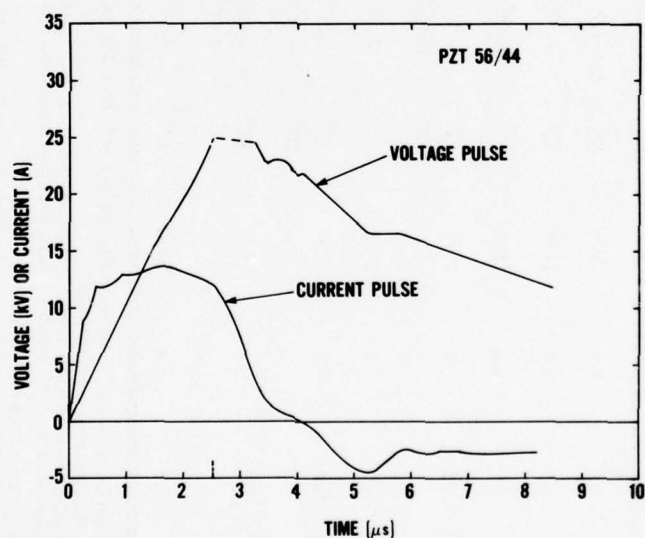


Figure 18. Voltage and current pulses for PZT 56/44 unit in Shot 83. The load capacitance was 1198 pF and the input shock stress was 6.4 GPa. The transit time for the depoling stress wave was taken to be 2.51 μ s. This is the time when the current pulse amplitude began to decrease significantly. The peak of the voltage pulse went off scale and was not recorded.

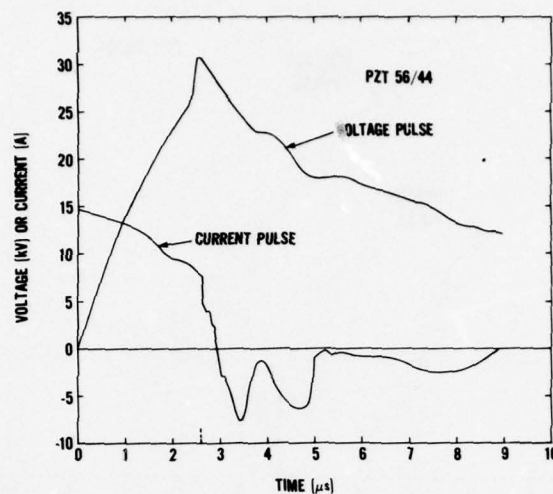


Figure 19. Voltage and current pulses for PZT 56/44 unit in Shot 84. The load capacitance was 1198 pF and the input shock stress was 7.8 GPa. The transit time for the depoling stress wave was taken to be 2.60 μ s. This is the time when the current pulse amplitude began to decrease significantly. The peak voltage of 27 kV was obtained by extrapolating the voltage prior to the sudden increase in amplitude to a value at transit time. The reason for the sudden increase in the voltage pulse just before transit time is not known.

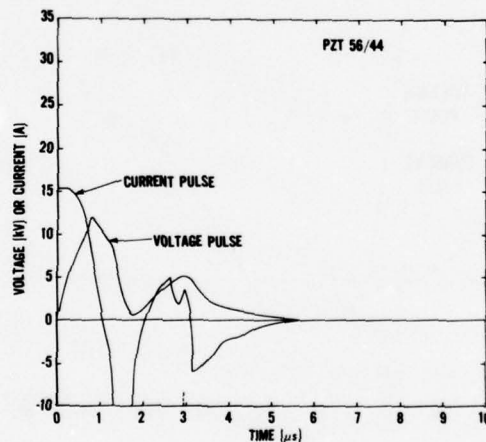


Figure 20. Voltage and current pulses for PZT 56/44 unit in Shot 85. The load capacitance was 1198 pF and the input shock stress was 11.8 GPa. An abrupt decrease occurred in the voltage pulse at 0.79 μ s indicating electrical breakdown in the PZT target assembly. After the voltage dropped to zero at about 1.80 μ s and the breakdown current was quenched, a second pulse occurred and peaked at about 2.93 μ s, the expected transit time for the depoling pulse. It is possible that the second pulse is due to a continued depoling of the unit coupled with the existence of a non-zero electrical breakdown threshold.

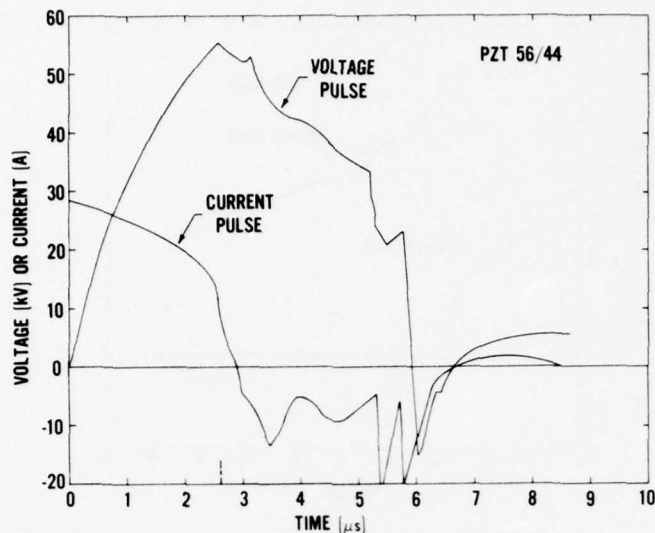


Figure 21. Voltage and current pulses for PZT 56/44 unit in Shot 87. The load capacitance was 1198 pF and the input stress was 7.9 GPa. The transit time as determined by the peak in the voltage pulse and the sudden decrease in the current pulse was 2.57 μ s. Electrical breakdown occurred in the target assembly between 5.2 and 6 μ s.

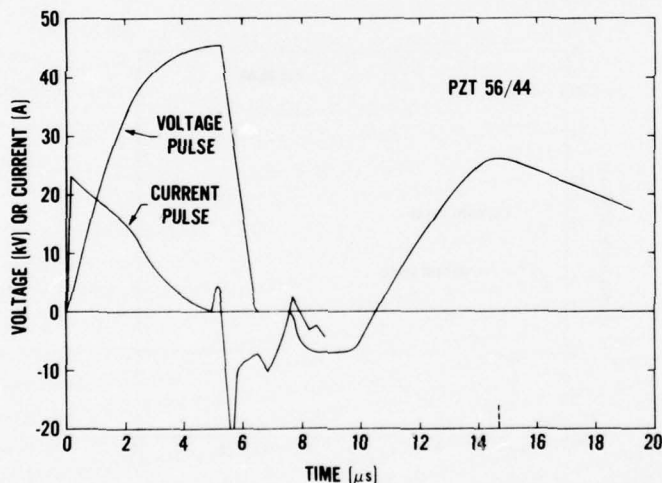


Figure 22. Voltage and current pulses for PZT 56/44 unit in Shot 121. The load capacitance was 1233 pF and the input stress was 7.9 GPa. Due to the length of this unit it experienced shock and relief wave interactions over much of the time duration of the depoling stress wave. Electrical breakdown occurred in the target assembly at 5.25 μ s. After the voltage dropped to zero and the breakdown current was quenched, a second pulse occurred which peaked at about 14.68 μ s and had an amplitude of about 60% of the first pulse. The recording time for the current pulse was about 9 μ s as compared with 19 μ s for the voltage pulse.

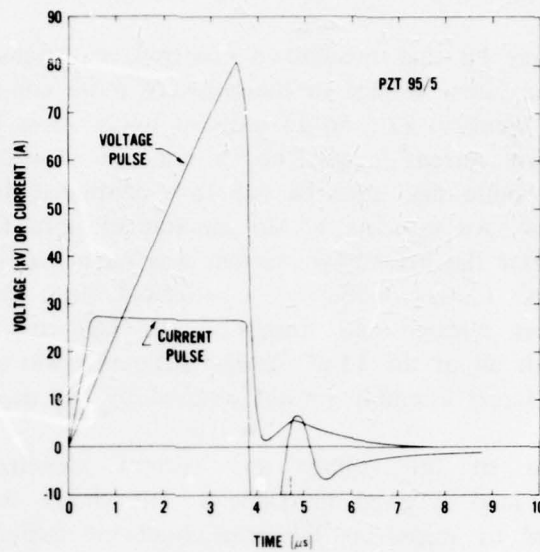


Figure 23. Voltage and current pulses for PZT 95/5 unit in Shot 122. The load capacitance was 1233 pF and the input stress was 2.9 GPa. For this shock stress the PZT 95/5 material responded essentially in an ideal manner before electrical breakdown occurred at 3.58 μ s. After electrical breakdown occurred and the voltage dropped to zero at 4.17 μ s a second pulse occurred and peaked at 4.74 μ s.

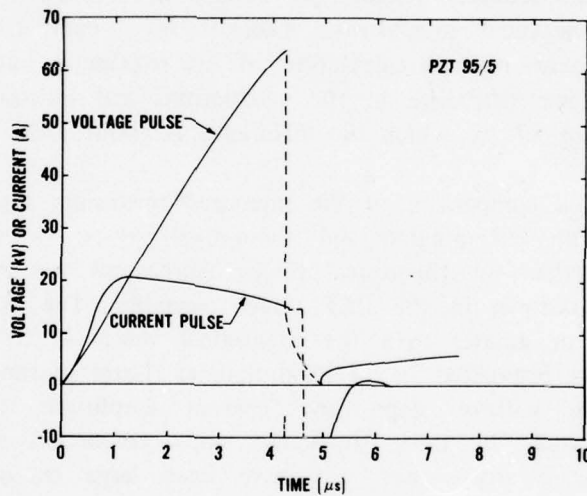


Figure 24. Voltage and current pulses for PZT 95/5 unit in Shot 123. The load capacitance was 1233 pF and the input stress was 1.4 GPa. Electrical breakdown in the target assembly occurred at 4.27 μ s. The dashed lines indicate that the pulses were not recorded during breakdown. After the voltage fell to zero at 4.97 μ s no noticeable recovery pulse occurred. This is probably because the depoling stress wave had already propagated through the unit.

123; the reason may be that breakdown occurred near transit time. In Shot 85 the 2.93 μ s time to maximum voltage in the recovery pulse compares favorably with the depoling times for identical PZT 56/44 units at lower stress levels. This suggests that after the breakdown current is quenched a non-zero electrical breakdown threshold exists. The second pulse may then be due to a continued depoling of the PZT unit by the shock wave. An estimate of the amount of unreleased charge on the PZT unit in Shot 85 after the breakdown current was quenched is 20 μ C. Of this charge approximately 7 μ C (corresponding to a measured peak voltage of 5 kV for the recovery pulse) was released and stored on the PZT and load capacitances. This means that some or all of the 13- μ C charge difference was either lost to breakdown conduction in the target assembly or not released by the depoling wave.

A comparison of the voltage and current measurements for the charge transferred to the load is given in Table 8. The charge transferred in the current pulses was obtained by measuring the area under the current-time profiles. For the three shots in which breakdown and recovery were observed the charge transferred before electrical breakdown and in the recovery pulse are listed. The values for voltage measurements (not including the recovery pulses) are on the average about 6% larger than those for the current measurements. For the recovery pulses the voltage measurements were about 50% larger than the current measurements. These differences for the recovery pulses may be due to the large current oscillations that occurred after electrical breakdown. Table 9 is a comparison of the maximum current measurements with a calculation of the maximum current from the voltage pulses. The average difference in the calculations and measurements is about 10%, not including Shot 87 for which the difference is about 50%.

Table 10 is a comparison of the measured maximum load voltage and released charge values with extrapolated and theoretical values. In all cases the measured values were less than the theoretical values. Agreement was good in Shot 122 prior to electrical breakdown in the PZT target assembly. The extrapolated values were either equal to or greater than the theoretical values in five shots indicating that initially the units responded in an ideal manner. Later in time the response became nonideal as the voltage slope and current amplitude decreased or electrical breakdown occurred. In three shots the units responded initially in a nonideal manner; the shock stress may not have been large enough to cause complete depoling.

Table 7 lists the maximum electric fields that were generated in the PZT units. These can be compared with the coercive fields in Table 3. For the PZT 56/44 material a maximum electric field of 2.1 kV/mm was generated in Shots 84 and 87. This is about 2.6 times the coercive field for this material. In comparison, the electric field before electrical breakdown in Shot 85 was 0.93 kV/mm. For the PZT

Table 8. Comparison of voltage and current probe measurements of charge transferred to capacitive load.

| Shot No. | Voltage Probe ^a (μC) | Current Probe ^a (μC) |
|----------|--|--|
| 71 | 28 | No Probe |
| 83 | 30 | 31 ^d |
| 84 | 33 | 31 ^d |
| 85 | 14 ^b 6 ^c | 12 ^b 3 ^c |
| 87 | 66 | 60 ^d |
| 121 | 56 ^b 32 ^c | 55 ^b No Measurement |
| 122 | 100 ^b 7 ^c | 96 ^b 2 ^c |
| 123 | 79 ^b | 71 ^b |

^aThese values include the charge transferred to the 0.91-m RG-213/U cable and, where appropriate, the capacitive voltage divider.

^bCharge transferred before electrical breakdown.

^cCharge transferred in recovery pulse.

^dIntegrated charge up to a time corresponding to an abrupt decrease in the current pulse amplitude.

Table 9. Comparison of maximum current measurements and calculations from voltage pulses.

| Shot No. | Maximum Current Measurement (A) | Maximum Current Calculation ^a (A) |
|----------|---------------------------------|--|
| 71 | No Probe | 13 |
| 83 | 14 | 13 |
| 84 | 15 | 17 |
| 85 | 16 | 20 |
| 87 | 28 | 43 |
| 121 | 23 | 25 |
| 122 | 28 | 30 |
| 123 | 20 | 21 |

^aCalculated from the equation $i = C_L(dV/dt)_0$ where C_L is the total load capacitance and $(dV/dt)_0$ is the initial slope of the voltage pulse. The capacitance and slope values were obtained from Table 7.

95/5 material a maximum electric field of 3.2 kV/mm was obtained in Shot 122 before electric breakdown occurred. This is about 2.9 times the coercive field for this material.

The maximum electric fields in Table 7 can also be compared with dielectric breakdown strength measurements under ambient conditions for PZT 65/35 material.⁸ (PZT 65/35 is a solid solution containing 65 mole % lead zirconate and 35 mole % lead titanate with niobium as a minor added constituent.) The breakdown strength is 3.7 and 2.9 kV/mm for PZT 65/35 material that is 3.2- and 6.4-mm thick, respectively. In our experiments the PZT elements were 3.2-mm thick in the first five shots and 6.4-mm thick in the last three shots. The shock-generated maximum electric fields were all less than the ambient-condition PZT 65/35 breakdown fields except in Shot 122. For this shot electrical breakdown occurred at 3.2 kV/mm for a shock stress of 2.9 GPa.

Table 10. Comparison of voltage measurements for the shock-depoled PZT units with calculations for the theoretical maximum voltage assuming ideal units.

| Shot No. | Maximum Load Voltage (kV) | | Charge Transferred to Load ^b (μC) | | | | Fraction of Available Charge Transferred to Load | | | | Released Charge ^c (μC) | | | | Fraction of Available Charge Released | |
|----------|------------------------------------|---------------------------|--|------------------------------------|------------------|-------------|--|------------------|-------------|-------------------------------------|-----------------------------------|-------------|--|-------------------|---------------------------------------|-------------|
| | Measured | Extrapolated ^a | Theoretical | Measured | Extrapolated | Theoretical | Measured | Extrapolated | Theoretical | Measured | Extrapolated | Theoretical | Measured | Extrapolated | Theoretical | Theoretical |
| 71 | 19 | 25 | 29 | 28 | 38 | 44 | 0.56 | 0.75 | 0.86 | 33 | 44 | 51 | 0.65 | 0.86 | 1.0 | |
| 83 | 25 | 27 | 35 | 30 | 32 | 43 | 0.58 | 0.63 | 0.83 | 36 | 38 | 51 | 0.70 | 0.75 | 1.0 | |
| 84 | 27 | 37 | 36 | 33 | 44 | 43 | 0.64 | 0.86 | 0.83 | 39 | 53 | 51 | 0.77 | 1.03 | 1.0 | |
| 85 | 12 ^d 5 ^e | 51 ^f | 37 | 14 ^d 6 ^e | 61 ^f | 44 | 0.27 ^d 0.12 ^e | 1.2 ^f | 0.83 | 17 ^d 7 ^e | 73 ^f | 53 | 0.33 ^d 0.14 ^e | 1.38 ^f | 1.0 | |
| 87 | 55 | 92 ^f | 71 | 66 | 110 ^f | 85 | 0.65 | 1.1 ^f | 0.83 | 80 | 132 ^f | 102 | 0.78 | 1.29 ^f | 1.0 | |
| 121 | 45 ^d 26 ^e | 214 ^g | 228 | 56 ^d 32 ^e | 264 | 282 | 0.11 ^d 0.06 ^e | 0.52 | 0.55 | 101 ^d 59 ^e | 476 | 508 | 0.20 ^d 0.12 ^e | 0.94 | 1.0 | |
| 122 | 81 ^d 6 ^e | 112 | 110 | 100 ^d 7 ^e | 138 | 135 | 0.71 ^d 0.05 ^e | 0.99 | 0.97 | 103 ^d 8 ^e | 143 | 140 | 0.74 ^d 0.05 ^e | 1.02 | 1.0 | |
| 123 | 64 ^d | 74 | 107 | 79 ^d | 91 | 132 | 0.58 ^d | 0.67 | 0.97 | 81 ^d | 94 | 136 | 0.60 ^d | 0.69 | 1.0 | |

^aThis voltage was obtained by extrapolating the initial slope of the measured voltage pulse to a value corresponding to the time to maximum voltage, or in the case of electrical breakdown, the time of maximum voltage for the recovery pulse. Values for the slope and time are given in Table 7.

^bIncludes the charge transferred to the 0.91-m RG-213/U cable and, where appropriate, the capacitive voltage divider.

^cSum of charge released to PZT unit and transferred to load. The charge released to the PZT unit was calculated by assuming that its capacitance (Table 3) did not change under shock compression and no charge was lost to conduction in the unit.

^dValue just before electrical breakdown.

^eValue in recovery pulse.

^fValue larger than for ideal response.

^gDetermined using the calculated time (10.8 μs) and not the measured time (14.7 μs) to maximum voltage. A value of 291 kV for the extrapolated voltage is obtained if 14.7 μs is used.

Table 7 also lists the maximum load energy, maximum load energy density and average power transferred to the load for each shot. For the PZT 56/44 material the maximum load energy and the average power transferred to the load are largest for Shot 87. The measured values for maximum load energy and maximum load energy density can be compared with theoretical values of 3.0 J and 0.38 J/cm³, respectively. The measured values are about 60% of the theoretical values. The theoretical values were calculated assuming the PZT unit in Shot 87 responded in an ideal manner. For the PZT 95/5 material the energy and power values are largest for Shot 122. The theoretical values are 7.4 J and 0.63 J/cm³ for the maximum load energy and maximum load energy density, respectively. The measured values are about 56% of the theoretical values. If electrical breakdown had not occurred in this unit the measured values would probably have been approximately equal to the theoretical values.

A comparison of the voltage outputs from identical PZT 56/44 units in the first four shots of the series is given in Figure 25. The initial pulse slope approximately doubled (Table 7) as the shock stress increased from 4.4 to 11.8 GPa. The maximum voltage was largest for the 7.8 GPa shot. Before electrical breakdown the 11.8 GPa shot had essentially the same pulse shape as the 7.8 GPa shot. Figure 26 is a plot of the released charge for these shots. It was assumed that the capacitance of the PZT 56/44 units did not change under shock compression. An increase in the released charge occurred (from 65% to 77%) as the shock stress was increased from 4.4 to 7.8 GPa. This suggests that electrical conduction is not increasing in this stress range. There was an approximate 50% reduction in the released charge due to electrical breakdown in the 11.8 GPa shot.

The effect of increasing the size of the PZT 56/44 units is shown in Figure 27. For a shock stress of 7.8 GPa the maximum load voltage doubled (27 to 55 kV) by doubling the charge available for release (51 to 102 μ C). The source capacitance for both units before shock compression was 238 pF. Figure 28 shows the voltage outputs as a function of shock stress for the PZT 95/5 units. The source capacitances for Shots 123 and 122 before shock compression were 38 and 43 pF, respectively. The slope of the voltage outputs increased as the shock stress was increased. For the 1.4 GPa stress the PZT unit was not completely depoled, but when the stress was increased to 2.9 GPa the unit was completely depoled and responded in an ideal manner before electrical breakdown occurred.

The voltage and current pulses in Figures 17 through 24 indicate that in all cases, except Shot 122, the charge flow from the PZT unit decreased as the depoling stress wave propagated through it. This is shown by a decreasing amplitude for the current pulses and a concave downward shape for the voltage pulses. Prior

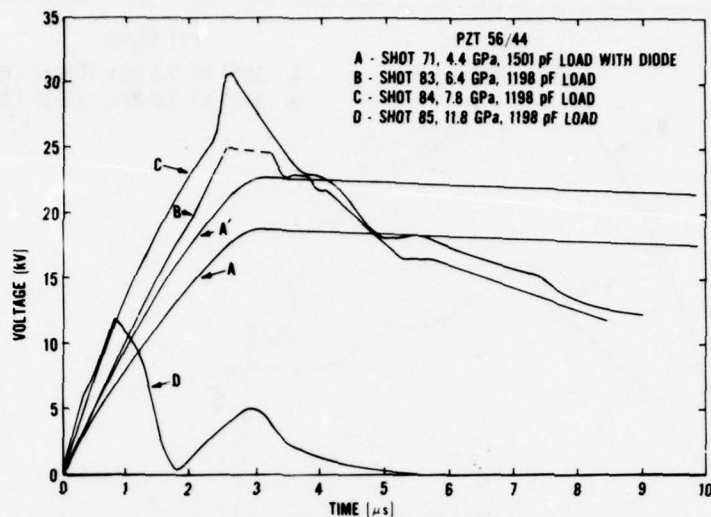


Figure 25. Voltage pulses as a function of shock stress for identical PZT 56/44 units. The units were cubes with an average side of 12.6 mm and an average initial capacitance of 241 pF. Curve A' is a recalculation of the voltage pulse for Shot 71 assuming a 1198 pF load capacitance for comparison with the other shots. The peak of curve B was off-scale on the oscilloscope record.

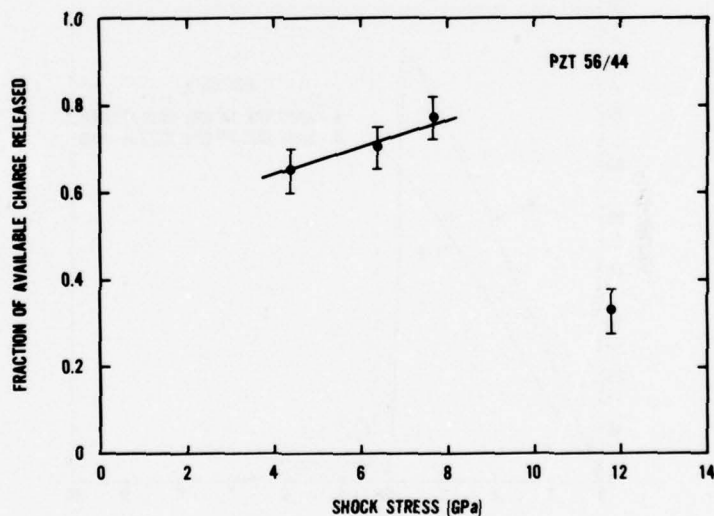


Figure 26. Released charge as a function of shock stress for identical PZT 56/44 units. The point for Shot 85 corresponds to the charge released before electrical breakdown in the target assembly. The released charge was determined from voltage measurements having estimated uncertainties of $\pm 5\%$. The available charge is $P_0 A$.

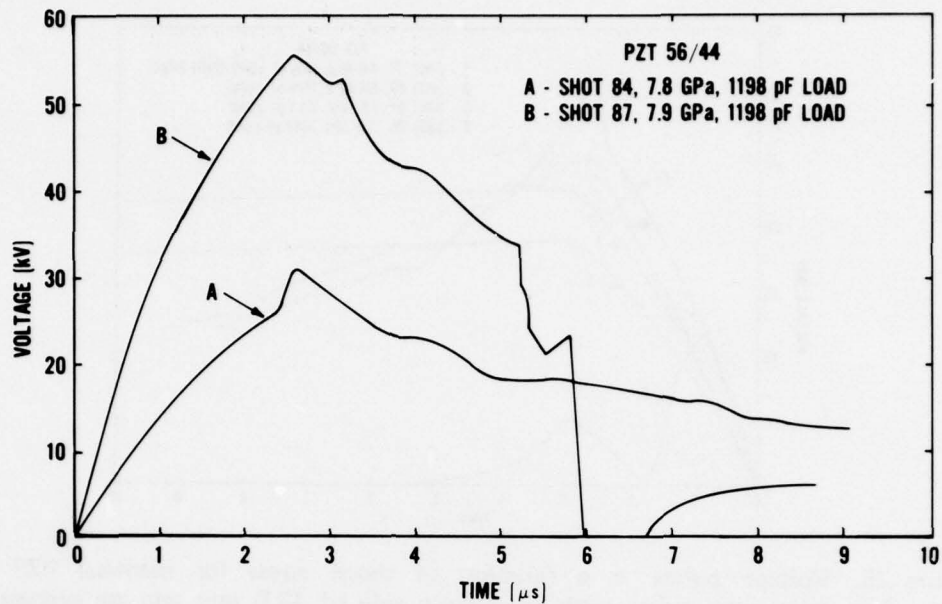


Figure 27. Effect of doubling the charge available for release on the voltage output for PZT 56/44 units.

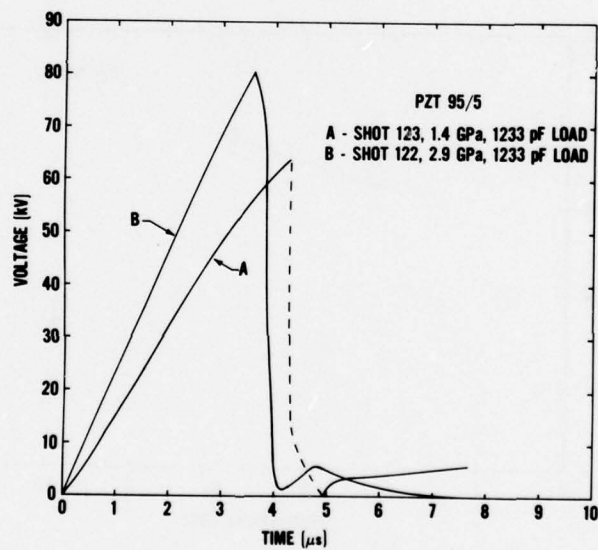


Figure 28. Voltage pulses for PZT 95/5 units. These rectangular units had an average initial capacitance of 41 pF. The dashed line indicates that curve A was not recorded during breakdown.

to the time of maximum load voltage these pulses are similar to those for the nonideal response in Figure 16(b). Figure 23 shows the voltage and current pulses for the PZT 95/5 Shot 122. These pulses indicate a linear voltage increase and a constant current amplitude prior to electrical breakdown. Note the similarity of these pulses with the ideal response pulses of Figure 16(a).

One contributing factor to the decreasing charge flow may be the increasing voltage on the PZT unit. This voltage increase may cause the bound surface charge to be more difficult to release, or may cause a repoling of the PZT material behind the shock front. Another contributing factor to the decreasing charge flow may be stress relief from the sides of the PZT unit behind the shock front since the unit is entirely encapsulated in a material of lower shock impedance. The 3.12-mm-thick brass electrodes on two sides of the unit would reduce this effect to some extent.

Figures 18, 19, and 21 show that for the PZT 56/44 Shots 83, 84, and 87 (prior to electrical breakdown) a decrease in the voltage amplitude occurred after the shock compression of the units. A repoling of the PZT units may be the reason for the decrease. This is suggested by the similarity in the shape of the decreasing voltage pulses for these shots. After shock compression, relief waves from the back surface of the impactor and from the PZT - epoxy interface would cause a reduction in the shock stress amplitude. The large PZT voltage coupled with this decreasing stress amplitude may cause repoling to occur.

Lysne and Percival⁹ have recently shown that the permittivity of PZT 95/5 decreased by about 50% at a shock stress of 1.4 GPa. If a decrease in the permittivity were the dominant effect in our data then the voltage pulses would show an increase in slope as the shock depoling wave propagated through the units. The PZT capacitance would be changed from a value corresponding to the uncompressed material to a smaller value corresponding to the compressed material. The effect of a 50% reduction in the source capacitance on the voltage pulses can be estimated. For the PZT 56/44 units (except Shot 121) and PZT 95/5 units the source capacitances were only about 20% and 3%, respectively, of the load capacitance; a 50% reduction in the source capacitance would reduce the circuit capacitance by only 8% and 2%, respectively. As the shock wave passed through the units this effect would cause an average increase in the slope of the voltage pulses of about 5% and 2%, respectively, for the PZT 56/44 and PZT 95/5 units. No uniform slope increases were observed, although in Shots 83 and 84 a voltage increase did occur just prior to shock transit time. A decrease in the permittivity may become more observable if the load capacitance were made smaller compared with the source capacitance; a change in the circuit capacitance, and therefore in the measured voltage, would be larger.

Table 11 gives the zero stress longitudinal and shear wave velocities for the materials. The value for the PZT 95/5 longitudinal wave velocity is in reasonable agreement with the PZT 95/5 depoling stress wave velocities in Table 7 indicating that the depoling stress wave corresponds to the elastic wave in this material. This is expected since the Hugoniot elastic limit for PZT 95/5 is approximately 4.0 GPa.²¹ Therefore, the 1.4 and 2.9 GPa PZT 95/5 shots correspond to the propagation of a single elastic wave in the material. In Section II it was stated that the PZT 95/5 material is located near the antiferroelectric PbZrO₃ phase boundary and was completely hydrostatically depoled with a stress of 0.29 GPa. Lysne⁴ has reported that under shock wave compression the PZT 95/5 (initial density 7.55 Mg/m³) ferroelectric-to-antiferroelectric phase transformation is complete for stresses above 1.6 GPa. This would explain the incomplete depoling observed in Shot 123 at a shock stress of 1.4 GPa. It would also explain the complete depoling prior to electrical breakdown that was observed in Shot 122 for a shock stress which was about twice the ferroelectric-to-antiferroelectric transformation stress.

Table 11. Summary of ultrasonic velocity measurements.

| Material | Density (Mg/m ³) | Longitudinal Wave Velocity ^a (km/s) | Shear Wave Velocity ^b (km/s) |
|-----------|---------------------------------|--|---|
| PZT 56/44 | 7.55 ^c | 4.52 ^d | 1.67 ^f |
| PZT 95/5 | 7.48 ^c | 4.40 ^e | 2.45 ^g |

^aMeasured for a nominal center frequency of 6 MHz of a broadband pulse.

^bMeasured for a nominal center frequency of 2 MHz of a broadband pulse.

^cAverage for two elements. The average element thickness was 6.47 mm.

^dAverage of six measurements.

^eAverage of eight measurements.

^fAverage of four measurements.

^gAverage of seven measurements.

The Hugoniot elastic limits for PZT 52/48 and PZT 65/35 are 1.9 and 3.6 GPa, respectively.^{20,6} Based on these results it is expected that a multiple-wave structure consisting of an elastic wave and at least one plastic wave was produced in the shock-depoled PZT 56/44 units since the shock stresses were all greater than 4.4 GPa. Comparing the depoling stress wave velocities for these shots (Table 7) with the 4.52 km/s ultrasonic longitudinal wave velocity suggests that the elastic wave is primarily responsible for depoling the PZT unit. This is also suggested by the results shown in Figure 26 since about 65% of the change has been released with a shock stress of 4.4 GPa and an additional charge release of only 12% is achieved when the shock stress is increased to 7.8 GPa.

Lysne and Bartel⁶ observed a ferroelectric-to-paraelectric phase change in axial-voltage-mode PZT 65/35 experiments at about 6 GPa. There was no strong evidence in our PZT 56/44 normal-voltage-mode experiments to indicate a ferroelectric-to-paraelectric phase change (such as a flat-topped current pulse that was observed in the 2.9 GPa PZT 95/5 shot). In the PZT 56/44 Shots 84 and 87 the amplitude of the current pulses decreased by about 50% during shock transit time.

VII. SUMMARY

PZT 56/44 and PZT 95/5 ferroelectric ceramics have been depoled in the normal mode using gas gun techniques. Nanofarad capacitors were charged in a few microseconds with electrical pulses having powers of hundreds of kilowatts. Complete charge release was not observed in any of the shots. This resulted from incomplete shock depoling of the PZT material or electrical breakdown and conduction in the units; relief wave interactions or the effects of voltage buildup on the depoling process may also cause incomplete charge release. The PZT 56/44 material was impacted in the stress range from 4.4 to 11.8 GPa. A maximum voltage of 55 kV was measured at 7.9 GPa with an associated charge release of 78%. This corresponds to a maximum load energy and maximum load energy density of 1.8 J and 0.22 J/cm³, respectively. These values are 60% of the calculated theoretical values. At 11.8 GPa shock-induced electrical breakdown occurred in the PZT 56/44 material. The PZT 95/5 material was impacted at 1.4 and 2.9 GPa stress levels. A maximum voltage of 81 kV and a charge release of 74% occurred at 2.9 GPa prior to electrical breakdown in the PZT material. This corresponds to a maximum load energy and maximum load energy density of 4.1 J and 0.35 J/cm³, respectively. These values are 56% of the calculated theoretical values.

REFERENCES

1. B. Jaffe, W. R. Cook, Jr., and H. Jaffe, *Piezoelectric Ceramics*, Academic Press, New York (1971).
2. W. Mock, Jr. and W. H. Holt, *Short-Circuit Current From the Axial-Mode Shock Depoling of PZT 56/44 Ferroelectric Ceramic Disks*, NSWC/DL TR-3781, Naval Surface Weapons Center, Dahlgren, Virginia (January 1978).
3. W. J. Halpin, *Current for a Shock-Loaded Short-Circuited Ferroelectric Ceramic Disk*, Journal of Applied Physics, Vol. 37, p. 153 (1966).
4. P. C. Lysne, *Dielectric Properties of Shock-Wave Compressed PZT 95/5*, Journal of Applied Physics, Vol. 48, p. 1020 (1977).
5. R. K. Linde, *Depolarization of Ferroelectrics at High Strain Rates*, Journal of Applied Physics, Vol. 38, p. 4839 (1967).
6. P. C. Lysne and L. C. Bartel, *Electromechanical Response at PZT 65/35 Subjected to Axial Shock Loading*, Journal of Applied Physics, Vol. 46, p. 222 (1975).
7. W. J. Halpin, *Resistivity Estimates for Some Shocked Ferroelectrics*, Journal of Applied Physics, Vol. 39, p. 3821 (1968).
8. P. C. Lysne, *Prediction of Dielectric Breakdown in Shock-Loaded Ferroelectric Ceramics*, Journal of Applied Physics, Vol. 46, p. 230 (1975).
9. P. C. Lysne and C. M. Percival, *Electric Energy Generation by Shock Compression of Ferroelectric Ceramics: Normal-Mode Response of PZT 95/5*, Journal of Applied Physics, Vol. 46, p. 1519 (1975).
10. J. T. Cutchen, *Polarity Effects and Charge Liberation in Lead Zirconate Titanate Ceramics Under High Dynamic Loads*, Journal of Applied Physics, Vol. 37, p. 4745 (1966).
11. The materials were purchased from Gulton Industries, Inc., Fullerton, California 92634.

12. This data was provided by Gulton Industries, Inc. The values in Table 1 are the averages of measurements on at least 10 pieces.
13. W. Mock, Jr. and W. H. Holt, *The NSWC Gas Gun Facility for Shock Effects in Materials*, NSWC/DL TR-3473, Naval Surface Weapons Center, Dahlgren, Virginia (July 1976).
14. This information was provided by R. Swyers of T&M Research Products, Inc., Albuquerque, New Mexico 87108.
15. The high voltage calibration measurements were performed by R. E. Hebner, Jr. of the High Voltage Measurements Section, Electricity Division, National Bureau of Standards, Washington, D. C. 20234.
16. R. A. Graham, *Piezoelectric Current from Shunted and Shorted Guard Ring Quartz Gauges*, Journal of Applied Physics, Vol. 46, p. 190 (1975).
17. *Selected Hugoniot*s, LA-4167-MS, prepared by Group GMX-6, Los Alamos Scientific Laboratory, Los Alamos, New Mexico (1969).
18. D. R. Christman, W. M. Isbell, S. G. Babcock, A. R. McMillan, and S. J. Green, *Measurements of Dynamic Properties of Materials, Vol. III, 6061-T6 Aluminum*, DASA 2501-3, General Motors Technical Center, Warren, Michigan (November 1971).
19. W. Mock, Jr. and W. H. Holt, *Shock Wave Compression of an Alumina-Filled Epoxy in the Low Gigapascal Stress Range*, Journal of Applied Physics, Vol. 49, p. 1156 (1978).
20. C. E. Reynolds and G. E. Seay, *Two-Wave Shock Structures in the Ferroelectric Ceramics Barium Titanate and Lead Zirconate Titanate*, Journal of Applied Physics, Vol. 33, p. 2234 (1962).
21. D. G. Doran, *Shock-Wave Compression of Barium Titanate and 95/5 Lead Zirconate Titanate*, Journal of Applied Physics, Vol. 39, p. 40 (1968).

APPENDIX A

**DISCUSSION OF ELECTRICAL EQUATIONS FOR THE
IDEAL RESPONSE OF A PZT UNIT WITH A
CAPACITIVE LOAD**

In Section V a simplified model was presented for the ideal and nonideal responses of a PZT unit. Equations for the charge release, voltage, and current were derived for these responses. Some of the equations that were derived in Section V are repeated here for completeness. In addition, the energy equations for the ideal response of a PZT unit are derived. Plots based on these equations and a discussion in terms of the load to source capacitance ratio C_L/C are provided.

At time t the charge release by the shock wave is

$$Q(t) = \begin{cases} P_0 A \frac{t}{\tau}, & 0 \leq t \leq \tau, \\ P_0 A, & t > \tau \end{cases} \quad (\text{A-1})$$

where τ is the shock transit time in the PZT unit. The charge on the PZT unit is

$$q(t) = \begin{cases} P_0 A \frac{C}{C+C_L} \left(\frac{t}{\tau} \right), & 0 \leq t \leq \tau, \\ P_0 A \frac{C}{C+C_L}, & t > \tau. \end{cases} \quad (\text{A-2})$$

The charge on the capacitive load is

$$q_L(t) = \begin{cases} P_0 A \frac{C_L}{C+C_L} \left(\frac{t}{\tau} \right), & 0 \leq t \leq \tau, \\ P_0 A \frac{C_L}{C+C_L}, & t > \tau. \end{cases} \quad (\text{A-3})$$

The voltage on the PZT unit and capacitive load is

$$V(t) = \begin{cases} \frac{P_0 A}{C+C_L} \left(\frac{t}{\tau} \right), & 0 \leq t \leq \tau \\ \frac{P_0 A}{C+C_L}, & t > \tau. \end{cases} \quad (\text{A-4})$$

Figure A-1 is a plot of the normalized charge $q(t)/(P_0A)$ and normalized voltage $V(t)/(P_0A/C)$ on the PZT unit. The charging region ($0 \leq t \leq \tau$) is characterized by a constant slope determined by the C_L/C ratio. For the open circuit case ($C_L/C = 0$) no charge is transferred to the load; all the released charge remains on the PZT unit. The charging region slope is P_0A/τ for the open circuit case. For the short circuit case ($C_L/C = \infty$) all the charge is transferred to the load at zero voltage.

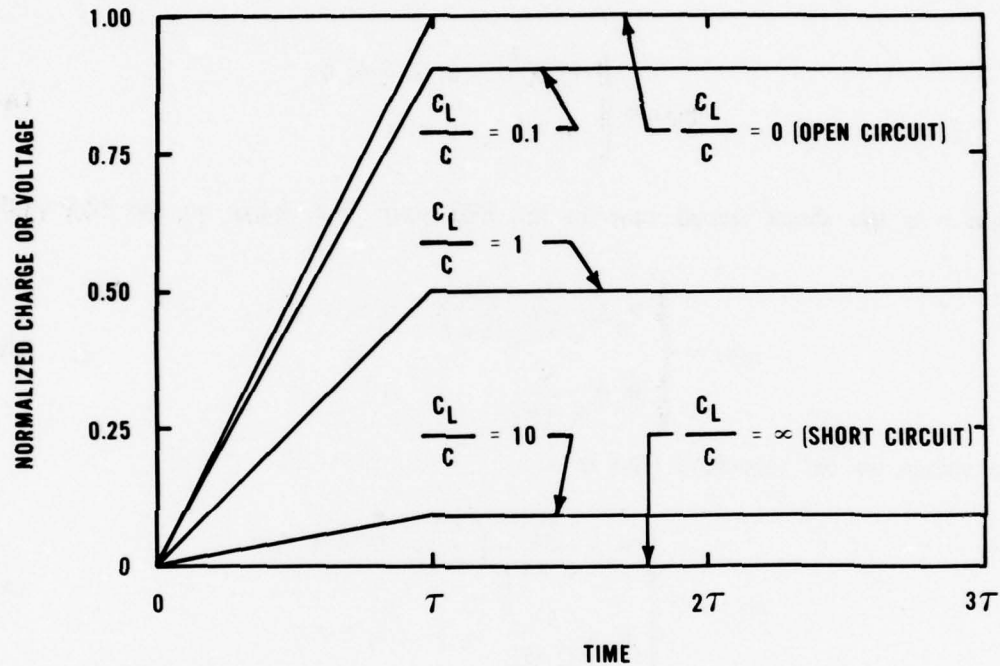


Figure A-1. Normalized charge and voltage on the PZT unit for various values of the C_L/C ratio.

The current is given by the equation

$$i(t) = \begin{cases} \frac{P_0A}{\tau} \frac{C_L}{C+C_L}, & 0 \leq t \leq \tau, \\ 0, & t > \tau. \end{cases} \quad (\text{A-5})$$

Figure A-2 is a plot of the normalized current $i(t)/(P_0 A/\tau)$. The current is a constant amplitude pulse for $0 \leq t \leq \tau$ and zero for $t > \tau$. For the short circuit case, the rate of charge release by the shock wave $P_0 A/\tau$ equals the amplitude of the short-circuit current pulse. The amplitude of the current pulse for a general load capacitor is a fraction of the short circuit current; the fraction is determined by the ratio of the load capacitance C_L to the total circuit capacitance.

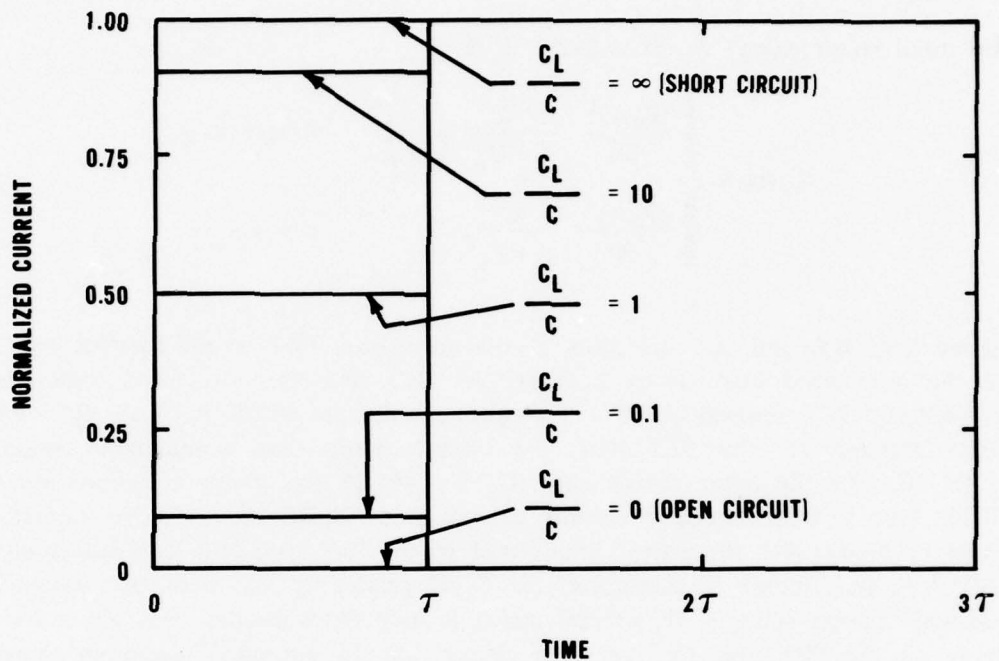


Figure A-2. Normalized circuit current for various values of the C_L/C ratio.

The energy on the PZT unit is given by

$$\mathcal{E}(t) = \begin{cases} \frac{(P_0 A)^2}{2C} \left(\frac{C}{C + C_L} \right)^2 \left(\frac{t}{\tau} \right)^2, & 0 \leq t \leq \tau \\ \frac{(P_0 A)^2}{2C} \left(\frac{C}{C + C_L} \right)^2, & t > \tau. \end{cases} \quad (\text{A-6})$$

The energy on the capacitive load is

$$\mathcal{E}_L(t) = \begin{cases} \frac{(P_0 A)^2}{2C} \frac{CC_L}{(C+C_L)^2} \left(\frac{t}{\tau}\right)^2, & 0 \leq t \leq \tau, \\ \frac{(P_0 A)^2}{2C} \frac{CC_L}{(C+C_L)^2}, & t > \tau. \end{cases} \quad (\text{A-7})$$

The total circuit energy $\mathcal{E}_T(t) = \mathcal{E}(t) + \mathcal{E}_L(t)$ is

$$\mathcal{E}_T(t) = \begin{cases} \frac{(P_0 A)^2}{2C} \frac{C}{C+C_L} \left(\frac{t}{\tau}\right)^2, & 0 \leq t \leq \tau, \\ \frac{(P_0 A)^2}{2C} \frac{C}{C+C_L}, & t > \tau. \end{cases} \quad (\text{A-8})$$

Figures A-3, A-4, and A-5 are plots of the normalized PZT energy $\mathcal{E}(t)/((P_0 A)^2/2C)$, and the normalized load energy $\mathcal{E}_L(t)/((P_0 A)^2/2C)$, and the normalized total energy $\mathcal{E}_T(t)/((P_0 A)^2/2C)$, respectively. For the open circuit case ($C_L/C = 0$) all the released charge remains on the PZT unit; the circuit energy has a maximum value of $(P_0 A)^2/2C$. For the short circuit case ($C_L/C = \infty$) all the energy equations are zero for all time t even though a current of magnitude $P_0 A/\tau$ flows in the circuit. As shown in Figure A-4 the energy transferred to the load capacitor is a maximum for $C_L/C = 1$, less energy is transferred for C_L/C greater or less than this value. This maximum energy value is $(P_0 A)^2/8C$ which is four times smaller than the maximum energy on the PZT unit for the open circuit case. In summary, maximum charge is transferred to the load for $C_L/C = \infty$, but maximum energy transfer occurs for $C_L/C = 1$.

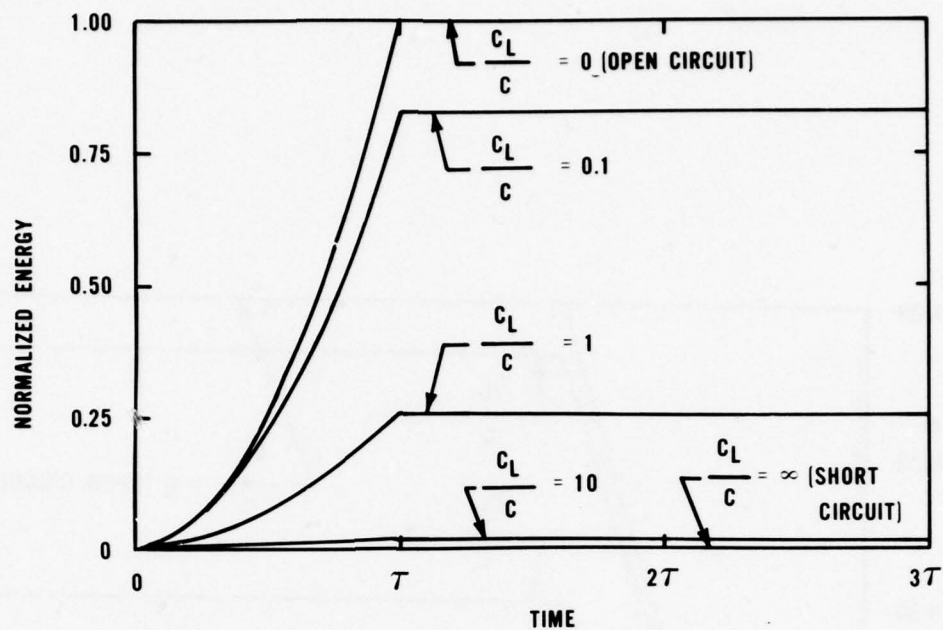


Figure A-3. Normalized energy on the PZT unit for various values of the C_L/C ratio.

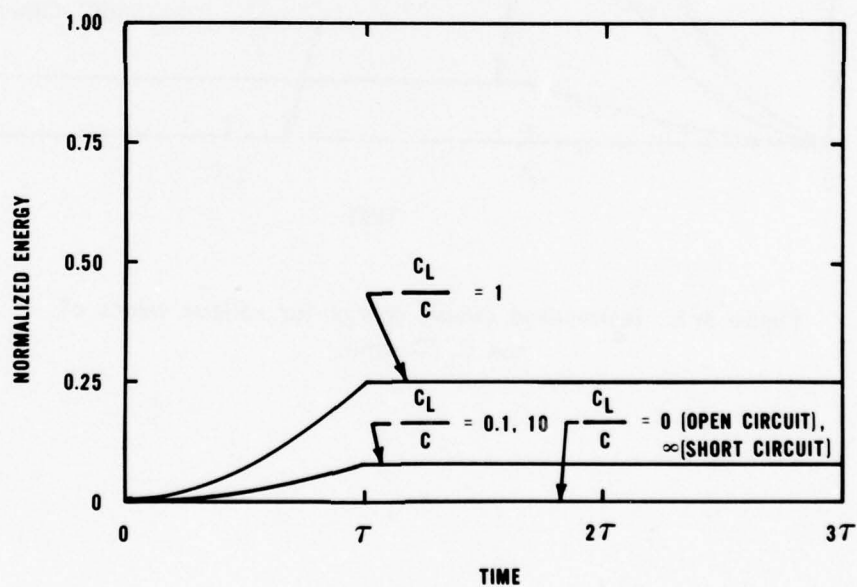


Figure A-4. Normalized energy on the load capacitor for various values of the C_L/C ratio.

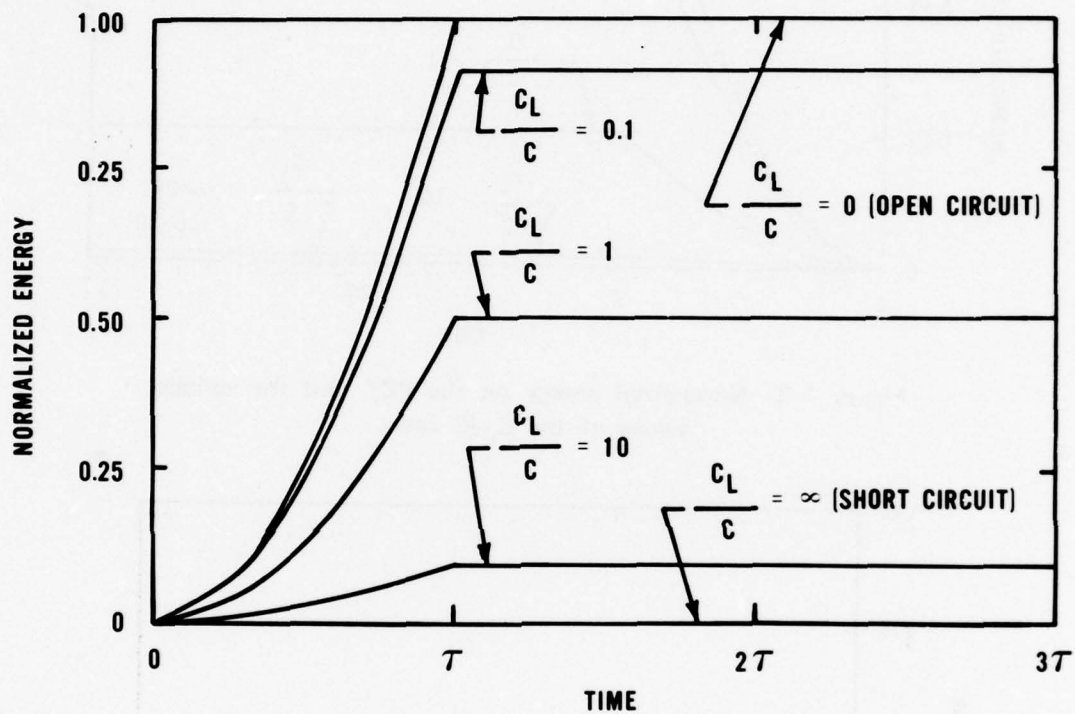


Figure A-5. Normalized circuit energy for various values of the C_L/C ratio.

APPENDIX B

VOLTAGE AND CURRENT OSCILLOSCOPE RECORDS

(The current oscilloscope records measured the charge transferred to 1097 pF lumped capacitor (Figure 2). To obtain the charge transferred to the total load capacitance the current pulse amplitudes must be multiplied by the ratio of total load capacitance (the 1097 pF lumped capacitor plus the 101 pF 0.97-m RG-213/U cable capacitance and, where appropriate, the 35 pF capacitance of the capacitive voltage divider) to the 1097 pF lumped capacitor. The current pulses in Figures 18 through 24 were obtained from the current measurements by this procedure.)

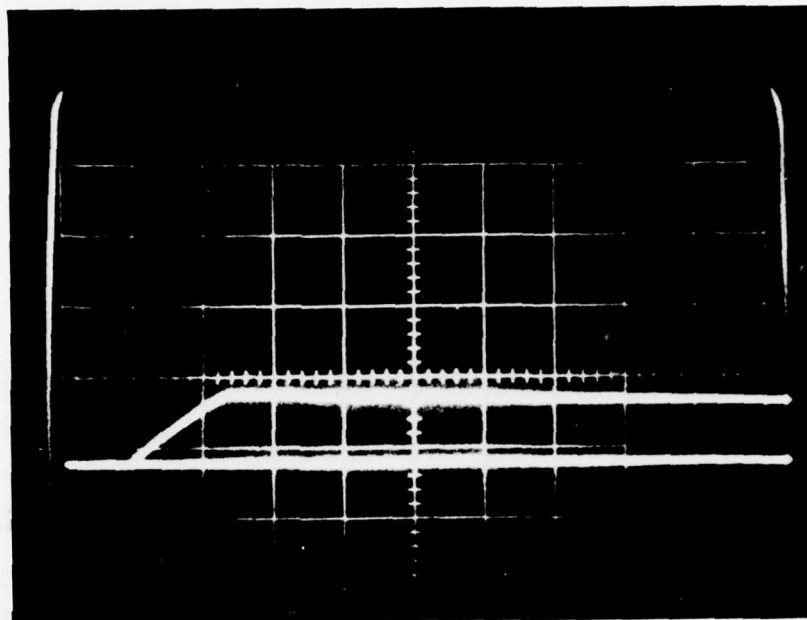
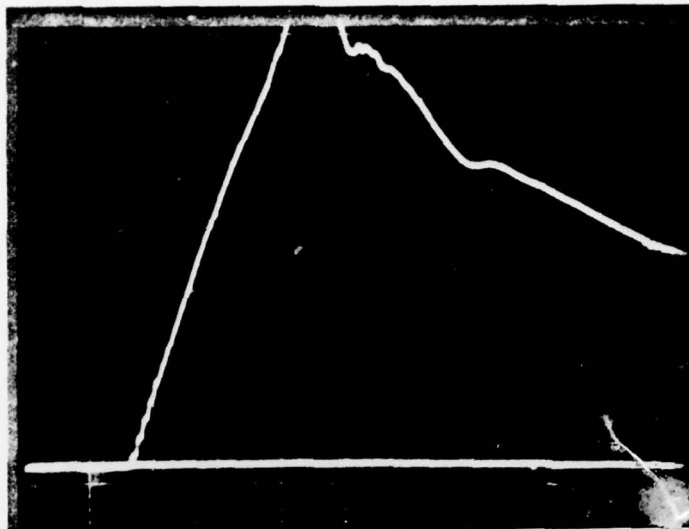
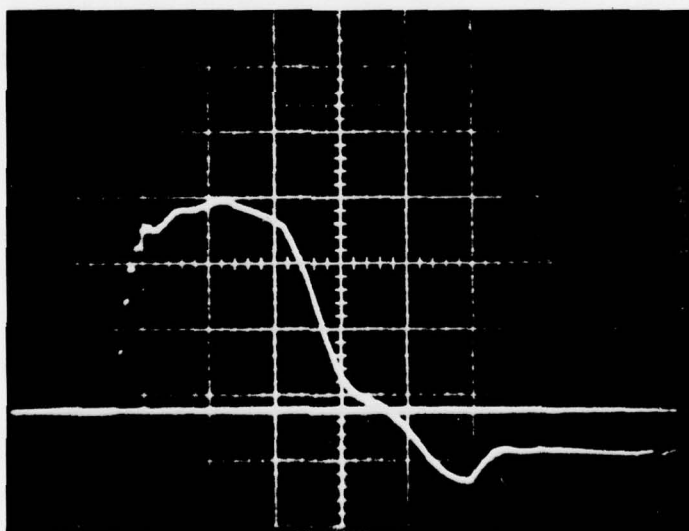


Figure B-1. Voltage record for Shot 71. The vertical scale is 19 kV/div and the horizontal scale is 2 μ s/div.

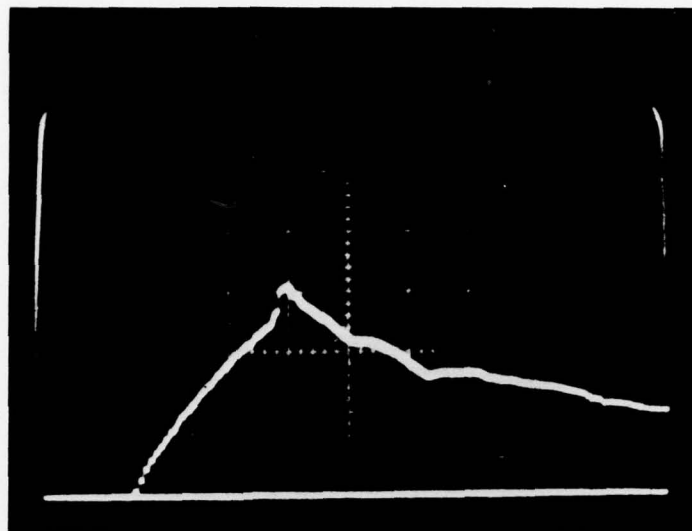


(a)

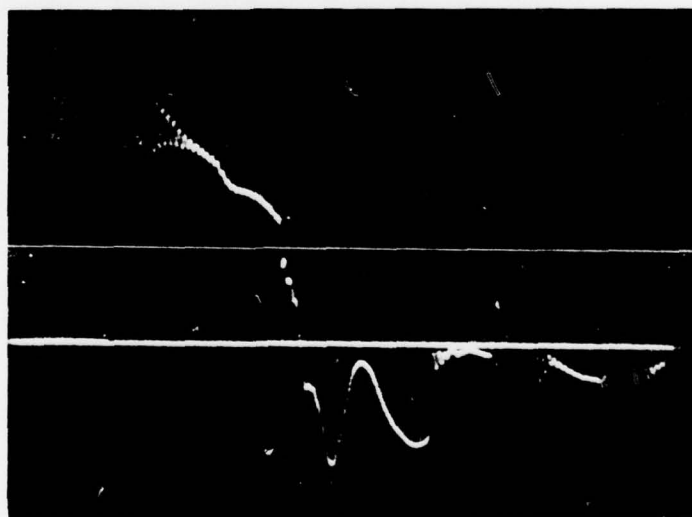


(b)

Figure B-2. Voltage and current records for Shot 83. (a) Voltage record. The vertical scale is 3.6 kV/div and the horizontal scale is 1 μ s/div. (b) Current record. The vertical scale is 4 A/div and the horizontal scale is 1 μ s/div.

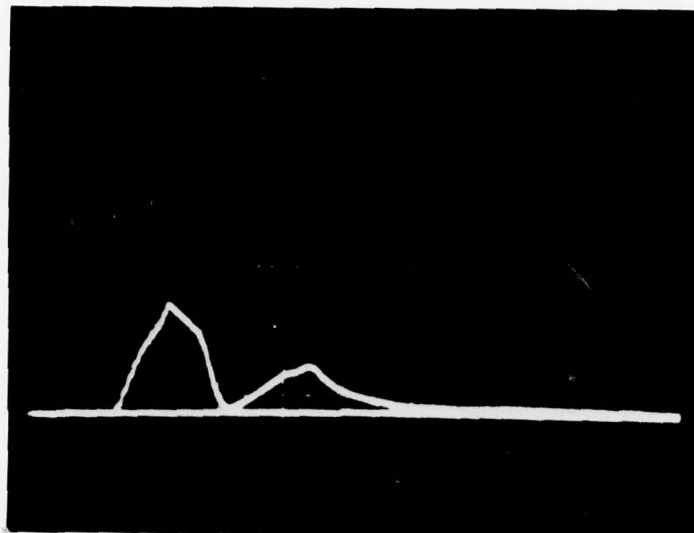


(a)

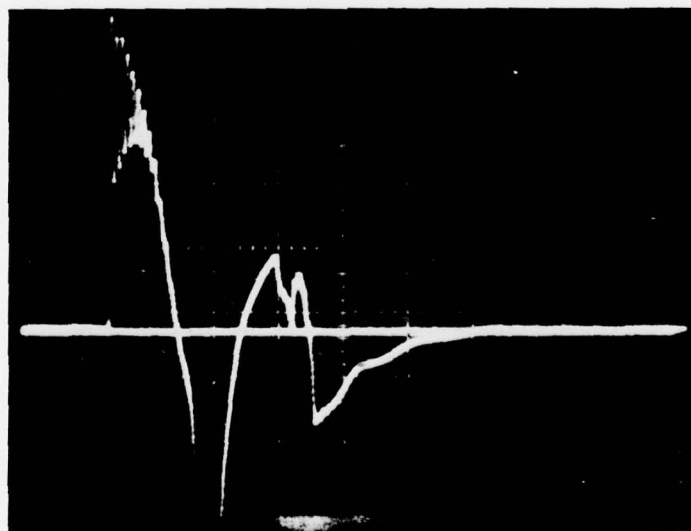


(b)

Figure B-3. Voltage and current records for Shot 84. (a) Voltage record. The vertical scale is 9 kV/div and the horizontal scale is 1 μ s/div. (b) Current record. The vertical scale is 4 A/div and the horizontal scale is 1 μ s/div.

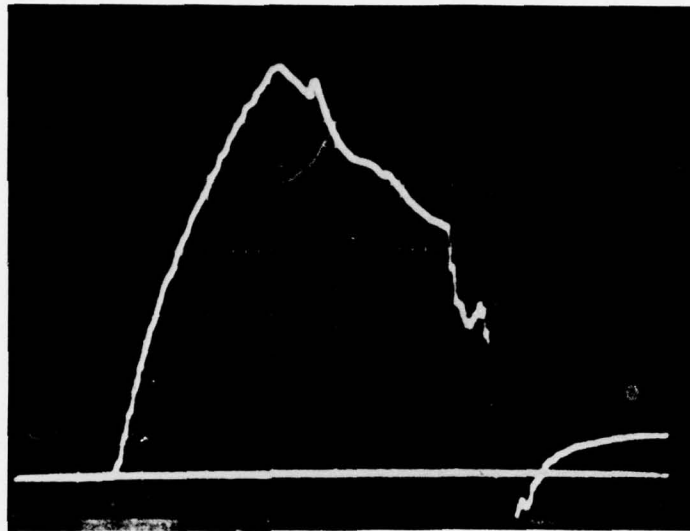


(a)

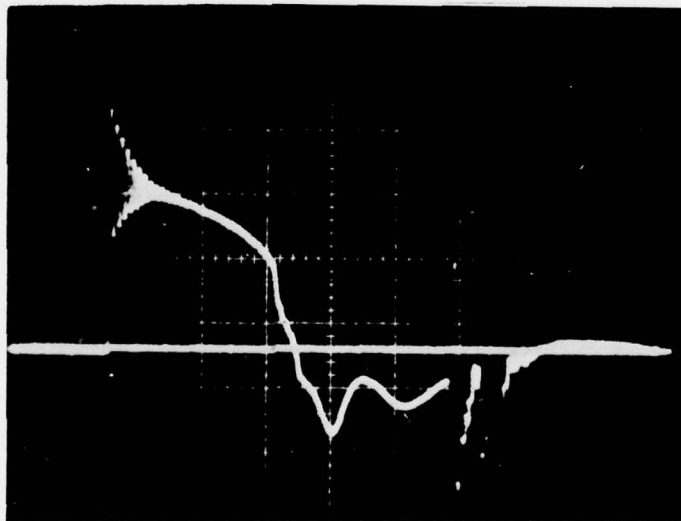


(b)

Figure B-4. Voltage and current records for Shot 85. (a) Voltage record. The vertical scale is 7 kV/div and the horizontal scale is 1 μ s/div. (b) Current record. The vertical scale is 4 A/div and the horizontal scale is 1 μ s/div.

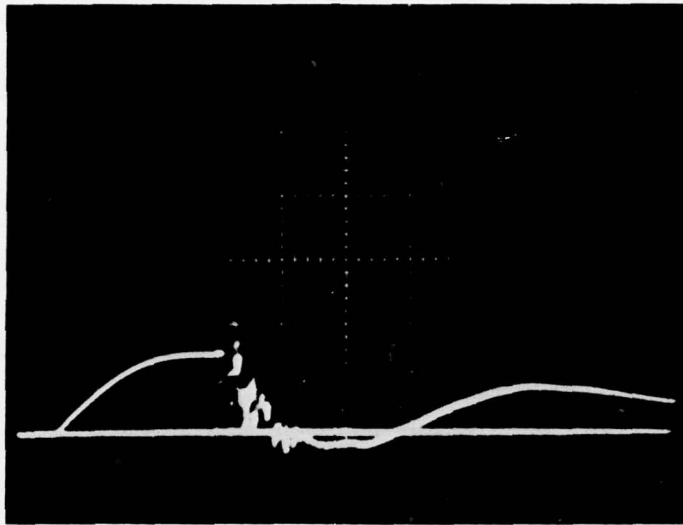


(a)

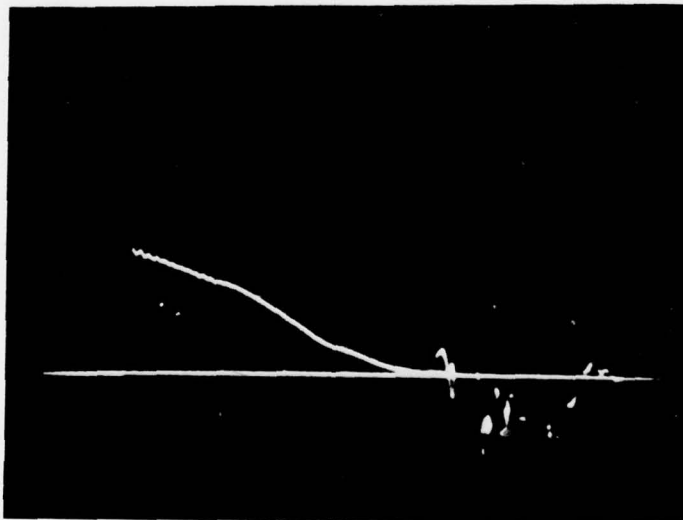


(b)

Figure B-5. Voltage and current records for Shot 87. (a) Voltage record. The vertical scale is 8.8 kV/div and the horizontal scale is 1 μ s/div. (b) Current record. The vertical scale is 10 A/div and the horizontal scale is 1 μ s/div.

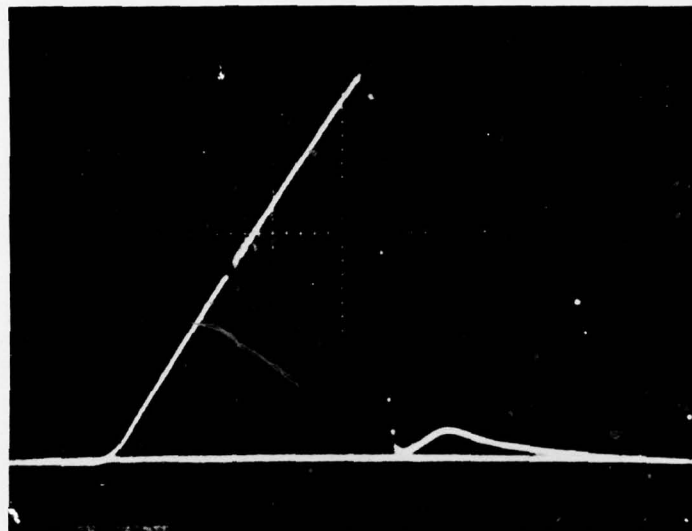


(a)

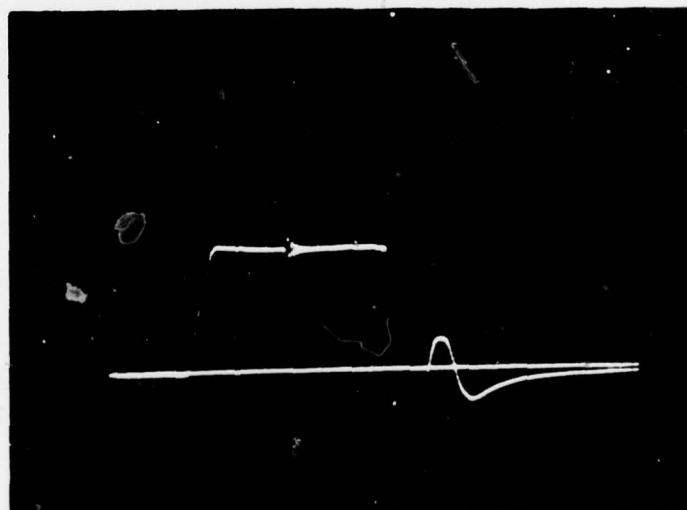


(b)

Figure B-6. Voltage and current records for Shot 121. (a) Voltage record. The vertical scale is 36.8 kV/div and the horizontal scale is 2 μ s/div. (b) Current record. The vertical scale is 10 A/div and the horizontal scale is 1 μ s/div.

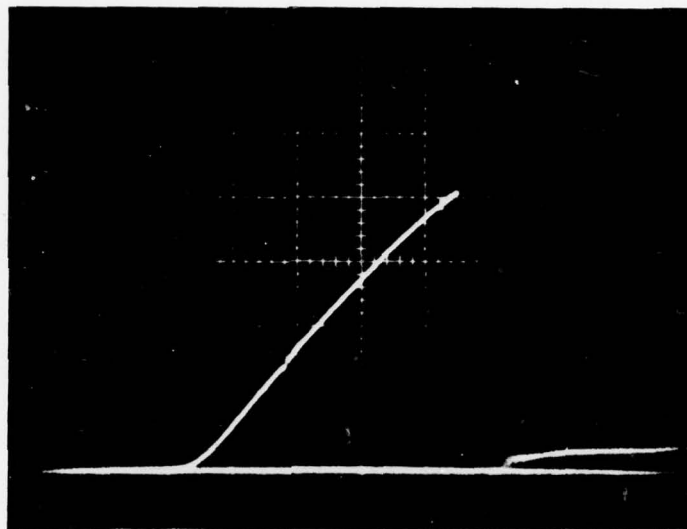


(a)

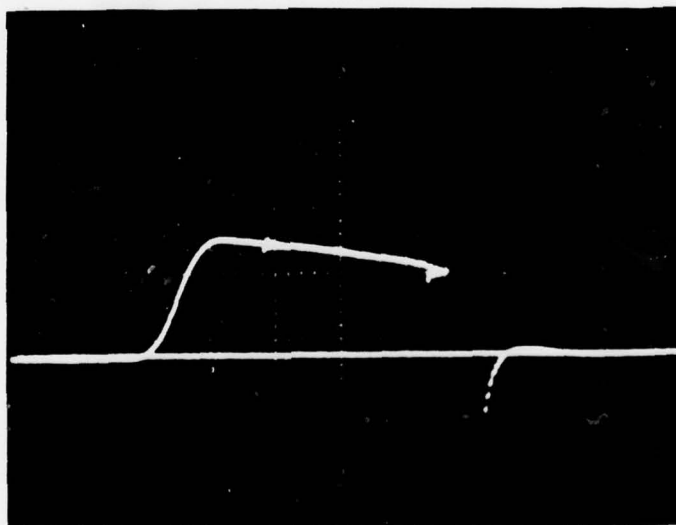


(b)

Figure B-7. Voltage and current records for Shot 122. (a) Voltage record. The vertical scale is 14.7 kV/div and the horizontal scale is 1 μ s/div. (b) Current record. The vertical scale is 10 A/div and the horizontal scale is 1 μ s/div.



(a)



(b)

Figure B-8. Voltage and current records for Shot 123. (a) Voltage record. The vertical scale is 14.7 kV/div and the horizontal scale is 1 μ s/div. (b) Current record. The vertical scale is 10 A/div and the horizontal scale is 1 μ s/div.

DISTRIBUTION

Commander
Naval Sea Systems Command
Washington, DC 20360
ATTN: SEA-03B S. R. Marcus
SEA-0331 S. J. Matesky
SEA-0332 W. W. Blaine
SEA-0332 R. A. Bailey
SEA-035 G. N. Sorkin
SEA-0352 M. A. Kinna
SEA-65313C L. H. Hawver

Commander
Naval Air Systems Command
Washington, DC 20360
ATTN: AIR-310A H. J. Mueller
AIR-310B J. W. Willis
AIR-320A T. F. Kearns
AIR-350 E. M. Fisher
AIR-350D H. B. Benefiel
AIR-5324 S. Englander

Office of Naval Research
Department of the Navy
Washington, DC 20360
ATTN: ONR-420 T. G. Berlincourt
ONR-465 E. I. Salkovitz

Office of Naval Research
536 S. Clark St.
Chicago, IL 60605
ATTN: George Sandoz

Office of Naval Research
Bldg. 114 Section D
666 Summer St.
Boston, MA 02210
ATTN: L. H. Peebles, Jr.

Commander
Naval Research Laboratory
Washington, DC 20375
ATTN: 6370 S. C. Sanday
6434 E. Skelton
7740 R. K. Parker
7908 W. Atkins
7908 A. Williams

Commander
Naval Weapons Center
China Lake, CA 93555
ATTN: M. E. Backman
S. A. Finnegan
J. Pearson
E. B. Royce

Superintendent
U. S. Naval Academy
Annapolis, MD 21402
ATTN: J. Fontanella

Director
Army Ballistics Research Laboratories
Terminal Ballistics Laboratory
Aberdeen Proving Ground, MD 20015
ATTN: W. S. deRosset
R. E. Franz
G. E. Hauver
G. Moss
R. Vitali

Commander
Army Materials and Mechanics Research Center
Watertown, MA 92172
ATTN: D. T. Dandekar
R. M. Lamothe
J. F. Mescall
P. V. Riffin

Commander
Army Research and Development Command
Dover, NJ 07801
ATTN: C. Christoe
C. deFranco
P. Harris
F. J. Owens

Commander
Harry Diamond Laboratory
Washington, DC 20438
ATTN: P. S. Brody

Los Alamos Scientific Laboratory
Los Alamos, NM 87544
ATTN: J. J. Dick
C. M. Fowler
J. M. Holt, Jr.
J. W. Hopson
J. N. Johnson
R. Morales
J. A. Morgan
B. W. Olinger
J. Wackerle
Technical Library

Sandia Laboratories
Albuquerque, NM 87115
ATTN: L. C. Bartel
B. M. Butcher
L. W. Davison
J. Gover
R. A. Graham
D. B. Hayes
R. J. Lawrence
P. C. Lysne
C. B. McCampbell
S. Montgomery
D. E. Munson
C. M. Percival
P. M. Richards
G. A. Samara

Lawrence Livermore Laboratory
University of California
Livermore, CA 94550
ATTN: D. L. Banner
S. Cochran
W. H. Gust
E. Nidick, Jr.
H. C. Rodean
J. Shaner

Shock Dynamics Laboratory
Washington State University
Pullman, WA 99163
ATTN: G. E. Duvall
G. R. Fowles

National Bureau of Standards
Washington, DC 20234
ATTN: R. A. MacDonald
D. H. Tsai

Seismological Laboratory
California Institute of Technology
Pasadena, CA 91125
ATTN: T. J. Ahrens

Stanford Research Institute
Poulter Laboratory
333 Ravenswood Avenue
Menlo Park, CA 94025
ATTN: D. Curran
D. C. Erlich
Y. Gupta
L. Seaman
D. Shockey

Defense Documentation Center
Cameron Station
Alexandria, VA 22314

Defense Printing Service
Washington Navy Yard
Washington, DC 20374

Library of Congress
Washington, DC 20540
ATTN: Gift and Exchange Division

(4)

Local:

C
D
E41
F
F10
F12
F12 (Luessen)
F12 (Berger)
G
G10
G13
G20
G30
G301
G31
G32
G33
G34
G35
G35 (Mock)
G35 (Holt)
G35 (Wishard)
G40
G50
G53
G531
G54
G60
R
R04
R10

R10 (Jacobs)
R11
R11 (Kamlet)
R13
R13 (Coleburn)
R13 (Erkman)
R13 (Forbes)
R13 (Roslund)
R30
R31
R31 (Augl)
R32
R33
R34
X210 (2)
X2101 (GIDEP) (2)